

Multi-dimensional teleoperation using EMG based impedance control with force feedback

Van Phan Cao



MASTERARBEIT

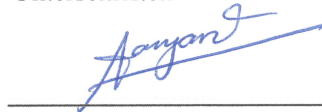
**MULTI-DIMENSIONAL TELEOPERATION
USING EMG BASED IMPEDANCE
CONTROL WITH FORCE FEEDBACK**

Freigabe:

Der Bearbeiter:

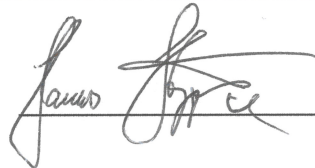
Unterschriften

Van Phan Cao



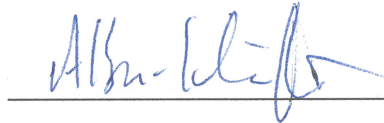
Betreuer:

Hannes Höppner



Der Institutsdirektor

Prof. Alin Albu-Schäffer



Dieser Bericht enthält 82 Seiten, 40 Abbildungen und 16 Tabellen

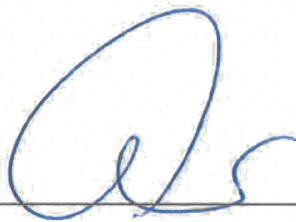
Multi-dimensional teleoperation using EMG based impedance control with Force Feedback

Nowadays, novel types of robotic systems are able to adjust in addition to an actively controlled impedance a passive intrinsic impedance, namely stiffness. Thus, similar to the human these robots are able to interact in an uncertain environment and change their compliance with respect to whatever is required by the task. In teleoperation, the electro-mechanical system which energetically connects an operator to a remote environment is often designed to be analogous to a light and rigid bar. If this is achieved, the force feedback is often regarded to be more faithful. However, the ability of impedance adaptability isn't used here.

In a recent work we have shown the benefits from an approach with force feedback that is able to additionally command human stiffness in 1 DoF using sEMG. The goal of this master thesis is to extend the prior work towards a multi-dimensional approach. Based on another thesis on measuring human arm stiffness in joint space using the lightweight robot LWR this work should continue with calibrating sEMG of the human arm with multi-dimensional Cartesian endpoint stiffness. The successful calibration will be applied to a multi-dimensional teleoperation approach with force feedback, e.g. in a track following task.

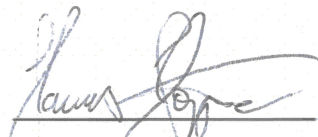
The thesis is structured as follows:

- Defining and implement a method to identify necessary inertial parameters
- Measure Cartesian endpoint stiffness of the human arm with the LWR and sEMG of the human of respective muscles simultaneously
- Calibrate stiffness with sEMG data in order to directly estimate stiffness by measuring muscle activation
- Use the mapping in a teleoperation approach with force feedback, where different sets of stiffness are required to successfully command the remote environment



Supervisor at TUD

Prof.Dr.-Ing. Bernd Kuhlenkötter



Supervisor at DLR

Dipl.-Ing. Hannes Höppner



Co-Supervisor at TUD

M.Sc. Maike Knöckner



INSTITUT FÜR PRODUKTIONSSYSTEME

DER TECHNISCHEN UNIVERSITÄT DORTMUND

Master Thesis in Automation and Robotics

More-dimensional teleoperation using EMG based impedance control with force feedback

Author: Cao, Van Phan
Supervisor: Univ.-Prof. Dr.-Ing. Bernd Kuhlenkötter
Advisor 1: Dipl.-Ing. Hannes Höppner
Advisor 2: M.Sc. Maike Klöckner
Date: March 31, 2014

Acknowledgments

I would like to express my deep gratitude to my family, my girl friend and Mrs. Dorothea Neumaier and Mr. Robert. They gave me immense support when I was doing this thesis.

Special thank goes to the Institute of Mechantronics and Robotics at German Aerospace center as well as the Institute of Production System at TU Dortmund for giving me the interesting topic of my master thesis. Especially, I am grateful to Prof. Bernd Kuhlenkötter and Ms. Maike Klöckner for supervising and revising my thesis.

I want to take this chance to thank all my friends Viet, Ribin, Jaeseok, Vikram, Markus, Maren and other friends at German Aerospace Center. Without their constant help and encouragement could have not come to completion.

Most importantly, the thesis could not be finished without patient and supportive instructions from my advisors, Mr. Hannes Höppner, Mr. Jordi Artigas, Mr. Claudio Castellini, Mr Marco De Stefano and other people in Bionics group at German Aerospace center. Mr. Hannes Hoepfner gave me a lot of helpful ideas in the task of measuring human arm stiffness. Additionally, he gave me motivation and took care of my personal life. Mr. Jordi Artigas and Mr. Marco gave me great ideas in designing force fields and in the task of teleoperation. And I got useful advices from Mr. Claudio Castellini on machine learning. Their friendliness and constructive supports all contributed greatly to the success and completion of my thesis. Working with them was a great experience in my life and very sincerely I want to send my deepest gratitude to all of them.

Abstract

Nowadays, novel types of robotic systems are able to adjust in addition to an actively controlled impedance a passive intrinsic impedance, namely stiffness. Thus, similar to the human these robots are able to interact in an uncertain environment and change their compliance with respect to whatever is required by the task. In teleoperation, the electro-mechanical system which energetically connects an operator to a remote environment is often designed to be analogous to a light and rigid bar. If this is achieved, the force feedback is often regarded to be more faithful. However, the ability of impedance adaptability is not used here. In a recent work we have shown the benefits from an approach with force feedback that is able to additionally command human stiffness in 1 DoF using sEMG. The goal of this master thesis is to extend the prior work towards a multi-dimensional approach.

Contents

Acknowledgements	ii
Abstract	iii
Outline of the Thesis	vi
1. Introduction	1
1.1. Motivation	1
1.2. Thesis structure	5
2. Theoretical background	7
2.1. Transformation	7
2.1.1. Homogeneous transformation [14]	7
2.1.2. Kinematic screw [14]	8
2.2. Cartesian impedance controller	10
2.2.1. Impedance controller concept	10
2.2.2. Kinematic singularity avoidance	12
3. Human Arm Identification	14
3.1. Geometrics Identification	14
3.1.1. The direct geometric model	14
3.1.2. The inverse geometric model [27]	18
3.1.3. Experiment setup and result	19
3.2. Inertial parameter identification	20
3.2.1. Formulation of the method	21
3.2.2. Experiment setup and result	23
3.2.3. Mass matrix in Cartesian coordinate	26
3.3. Stiffness identification	26
3.3.1. Human arm dynamic model in Cartesian coordinate	26
3.3.2. The experiment setup	28
3.3.3. Data processing	36
3.3.4. Results and discussion	38
4. Calibration of human arm stiffness and surface EMG signals	42
4.1. EMG processing	42
4.2. Least Squares Regression	45
4.2.1. Concept	45
4.2.2. Application of Least Squares Regression	46
4.2.3. Online estimation of arm stiffness	47

4.3. Regularized Least Squares	48
4.3.1. Concept	48
4.3.2. Application of Regularized Least Squares	48
4.3.3. Online estimation of the arm stiffness	50
4.4. Linearisation the stiffness matrix according to the sum of EMG signals	53
5. Teleoperation	54
5.1. The model of the teleoperation system	54
5.2. Implementation	54
5.2.1. Coordinate Transformation in teleoperation	55
5.2.2. Force feedback	56
5.2.3. Controller design for master robot	57
5.2.4. Controller design for slave robot	57
5.3. Results and discussions	58
6. Conclusion and future works	60
Appendix	63
A. Results of geometric identification	63
B. Calculation of Roll-Pitch-Yaw angles from rotational matrix	64
Bibliography	68

Outline of the Thesis

CHAPTER 1: INTRODUCTION

CHAPTER 2: THEORETICAL BACKGROUND

CHAPTER 3: HUMAN ARM IDENTIFICATION

CHAPTER 4: CALIBRATION OF HUMAN ARM STIFFNESS AND EMG SIGNALS

CHAPTER 5: TELEOPERATION

CHAPTER 6: CONCLUSION AND FUTURE WORK

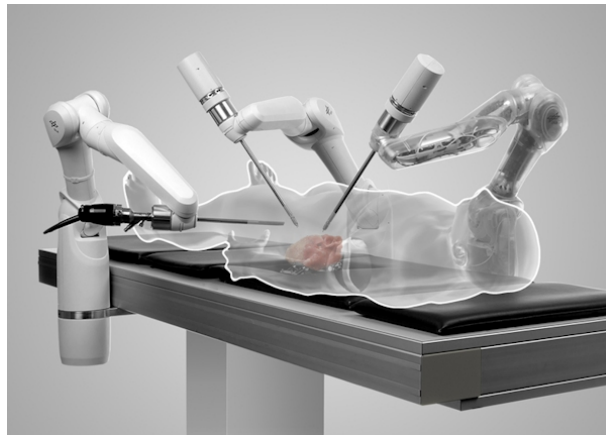
1. Introduction

1.1. Motivation

From the beginning of technology era humans had desire to interact and explore the world not only around them but also the places far away like in the sea or space where it is difficult to reach due to limitations in physical conditions of human. Tele-operation systems have been developed to elongate the human arm to unlimited space, satisfying their demands of better interacting with the world, better servicing, and more than ever making life better. Care-o-bot 3 which you can see in Fig. 1.1a is an assistant robot which is be-



(a) The Care-o Robot [1]



(b) MiroSurge Robotic system in DLR [19]

Figure 1.1.: Tele-manipulation applications

ing developed at Fraunhofer institute. This robot when necessary will be tele-operated to better assist old people in their house. MIRO [19] in Fig. 1.1b is a surgical robotic system that the operator control every deliberate movement of tele-surgery. DEOS is another ongoing research project in German Aerospace Center which is served in the space to grasp broken satellites as can be seen in Fig. 1.2. In such interactive applications, all the tasks to a certain extent require human in the control loop due to unknown and unstructured environment where robots themselves cannot handle by pre-programming. The question would be which properties such those systems should have. Firstly, it is intuitive that in order to effectively interact with the unknown environment the humans have to sense it to a certain extent like visual sensing or feeling of interaction with the environment in force or torque level. Secondly, how the human control the interaction in an efficient way. Those requirements originated the *bilateral tele-operation* architecture that enables human to remotely *sense* and remotely *act*. In other words, it is like bringing the remote environment to the human and bringing human to the remote environment through *bilateral tele-operation*



Figure 1.2.: The simulation of DEOS project [6]

system. Up to now the interaction aspect in *bilateral tele-operation* is only restricted in controlling the velocity or the position of the remote devices. That means technically the human/operator in some ways commands the position or velocity to the operated device. However the requirement of tele-operation in some special tasks is far more complicated. The project DEOS at DLR is about controlling a robot to catch broken satellites in space. Such deliberate tasks need carefully controlling the interaction and stabilizing the coupling system. In order to figure out an efficient way of controlling interaction, the movement in nature deserves a much careful consideration.

Nature has its own magic and powerful way to create *unliving* and *living* things and make them adapting and nourishing from time to time. Water, air, trees, animals and humans, etc ... all possess amazing properties to adapt themselves to their environment. From motion control point of view, it can be seen that mechanical properties of things have various characteristics. Water and air with extreme flexibility and fluidity are able to move harmoniously and autonomously according to their environment. They use their own intrinsic properties in combination with external force such as gravity to move. But turning to movements in animals we can observe that their movements are done somewhat purposely with regulation from their brain. A typical example of coordination and controlling motions in animal world is the movement of a cat when it is released from a high altitude. It seems to show us that the intrinsic dynamics is used more to generate such beautiful smooth movements [33]. The coordination of all parts of the body, gravity and the purpose of moving are harmoniously established. And it will be incomplete if abundance of human activities such as dancing, walking, swimming, driving a bike, playing piano, martial art and so on is not taken into account. Humans with high capability of learning can do much more complicated and difficult tasks. For example, when driving a bicycle on a flat road the driver has to keep his steering stronger in order to counteract the disturbing

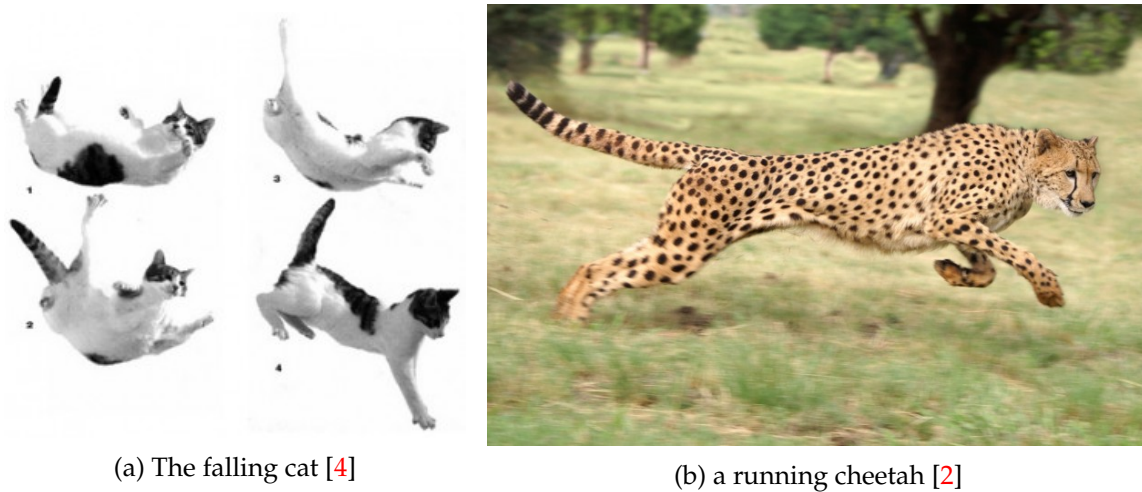


Figure 1.3.: The animal motions

force caused by the stones on the road. Another typical example is in winter when walking on a slippery road due to ice the legs are voluntarily controlled stiffer to avoid slipping. These situations seem to indicate that the humans change the limb stiffness to stabilize the system. Interestingly, when playing guitar the player can translate his emotion to a way to handle the strings to produce the emotional sounds. And now it gives rise to a question which rules are behind those movements and how we can extract those informations and transfer into tele-operation domains.

Many investigations of mechanical properties of tissue of human limbs have been done in order to have a deep insight into human movement control. In biomechanics, the mechanical properties of muscle and tendon have been studied. The physiologist Archibald Vivian Hill researched the elasticity and viscosity of muscle and gave out the Hill's elastic muscle models [12]. In Zoology, the storage of elastic strain energy in muscle and other tissues was studied by Alexander [11]. It turned out that tendon is the main sort of storing elastic energy that helps saving significant amount of energy during movements like running, jumping and insect flight [11]. In terms of control, many phenomena including stretch reflex, spinal reflex and long-latency reflex also have been researched to have more understanding of neuromuscular system. Mussa Ivaldi [28] had developed a very well-known method to measure and represent the field of elastic force associated with the postures in the plane. Consequently the hypothesis of virtual trajectory [22] has been proposed and applied in the controller design. This resulted in impedance controller implementation in robotics [29]. Most recently, Franklin have investigated the changes of human arm stiffness due to different disturbance force field [17]. The results showed that in an unstable environment, the change in joint stiffness is independent of the change in joint torque while in the stable environment changes in endpoint stiffness were well correlated with changes in joint torque [16]. That means the central nervous system (CNS) can modulate the impedance of the human arm by co-contraction of selective muscles in order to compensate for unstable dynamics while generating task-oriented forces. In realization of human control principles, DLR lightweight robot was developed in order to assist humans in various applications such as safely physical cooperating in assembly tasks or to



Figure 1.4.: The human motions

behave in human environment like Justin robot as can be seen in Fig. 1.5. In such inter-

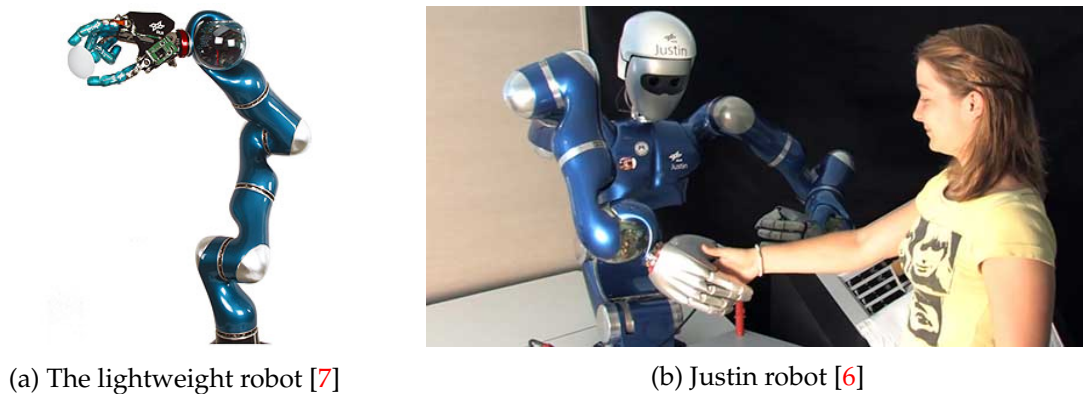
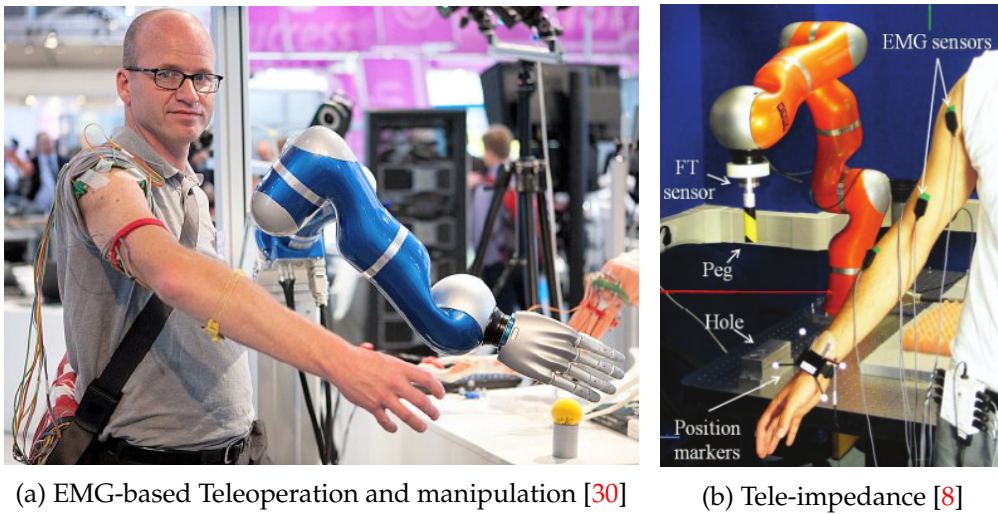


Figure 1.5.: The interaction control in robots

active and cooperative applications, the controller aspect have been studied in [10] [9] [29].

Along with those researches, surface *Electromyography* (sEMG) signal was investigated to extract useful information about arm motion such as the human arm kinematic, the grasping force or the human stiffness [32] [34] [31]. In [30] Vogel used sEMG signal to decode the human arm configuration in order to teleoperate the DLR lightweight robot. In addition, in [25], Hyun can extract joint stiffness from EMG signals and joint motion data by using artificial neuron network. The results showed that the sEMG signal becomes one of realizable means for estimating the human arm motion and human mechanical properties. Most interestingly, in [8] *tele-impedance* has been implemented to make the control of the slave robot more natural as illustrated in figure 1.6a. The *Electromyography* signals were used to extract the stiffness to control the lightweight robot. It is quite promising in



(a) EMG-based Teleoperation and manipulation [30]

(b) Tele-impedance [8]

Figure 1.6.: EMG-based control

some tasks like pegging in hole or catching a ball that with the tunable impedance from human the robot can fulfil the task more effectively. But the drawback of the implemented approach is that the calibration method is at one position while the human arm stiffness depends highly on the arm configuration. Moreover, the operator has no force feedback which limits the effectiveness of interacting. In MIRO project in DLR, the reliable bilateral control loop was developed that gives the operator the sense of interacting force during telesurgery.

By taking advantageous properties of human neuromuscular system into bilateral teleoperation, it can be expected that the performance of master-slave tele-operation systems for unknown environment will be improved. Those properties can be observed through the surface *Electromyography* signal that is easy to mount and non-invasive. The human arm impedance will be measured indirectly from EMG signals in real-time. Then this impedance will be sent to slave robot. In this fashion the slave robot can imitate the human operator in terms of mechanical properties at the wrist of the operator after the operator *feel* the remote environment through the visual and force feedback and act correspondingly to the current situation. Based on this idea, the goal of this thesis will be constructed as following:

- Measuring human arm stiffness in 2D
- Using machine learning to map EMG data and endpoint human arm stiffness
- Teleoperation using human-like impedance controller.

1.2. Thesis structure

The work comprises of 6 chapters. After introduction about the motivation and the goal of the thesis in chapter 1, chapter 2 describes the theoretical ground for the whole thesis. Then chapter 3 addresses human arm identification. This chapter includes geometrics, inertial

1. *Introduction*

parameters and endpoint stiffness identification of human arm. Subsequently, in chapter 4 calibration of human arm stiffness and EMG signals will be presented with 2 methods *Least Squares Regression* and *Regularized Least Squares*. Additionally, a simple method to scale stiffness according to EMG signals is also given. Chapter 5 contains teleoperation with force feedback. Finally, conclusion and future work are given in chapter 6.

2. Theoretical background

2.1. Transformation

In design and control of the robotic system, transformation of frame, vector and forces are of computational importance. In this chapter such kind of transformations will be presented in details which build the basis for the next chapters.

2.1.1. Homogeneous transformation [14]

Transformation of frames

The transformation from frame $\{A\}$ to frame $\{B\}$ is described by the (4×4) homogeneous transformation matrix ${}^A T_B$ which comprises translation and rotation such that:

$${}^A T_B = [{}^A s_B \ {}^A n_B \ {}^A a_B \ {}^A P_B] = \begin{pmatrix} s_x & n_x & a_x & P_x \\ s_y & n_y & a_y & P_y \\ s_z & n_z & a_z & P_z \\ 0 & 0 & 0 & 1 \end{pmatrix}, \quad (2.1)$$

where ${}^A s_B$, ${}^A n_B$ and ${}^A a_B$ are the unit vectors along the x_B , y_B and z_B projected in frame $\{A\}$ while ${}^A P_B$ is the coordinate of the origin of frame $\{B\}$ in frame $\{A\}$. The matrix ${}^A T_B$ can be interpreted as representing the frame $\{B\}$ in the frame $\{A\}$.

Transformation of vectors

Suppose that ${}^B P$ is the homogeneous coordinates of the point P in frame $\{B\}$, then the homogeneous coordinates of P in frame $\{A\}$ will be as follows:

$${}^A P = {}^A O_A P = {}^A O_A O_B + {}^A O_B P = {}^A P_B + {}^A s_B {}^B P_x + {}^A n_B {}^B P_y + {}^A a_B {}^B P_z = {}^A T_B {}^B P \quad (2.2)$$

Translational and rotational transformation matrices

Translation a, b and c along axes x , y and z respectively is represented by transformation matrix $Trans(a, b, c)$. We see that the orientation is not varying. Therefore, the transformation is described as:

$${}^A T_B = Trans(a, b, c) = \begin{pmatrix} 1 & 0 & 0 & a \\ 0 & 1 & 0 & b \\ 0 & 0 & 1 & c \\ 0 & 0 & 0 & 1 \end{pmatrix}. \quad (2.3)$$

2. Theoretical background

Let $Rot(x, \theta)$, $Rot(y, \theta)$ and $Rot(z, \theta)$ be the transformation matrices of a rotation around x , y and z an angle θ respectively we have:

$${}^A T_B = Rot(x, \theta) = \begin{pmatrix} 1 & 0 & 0 & 0 \\ 0 & C\theta & -S\theta & 0 \\ 0 & S\theta & C\theta & 0 \\ 0 & 0 & 0 & 1 \end{pmatrix} \quad (2.4)$$

$${}^A T_B = Rot(y, \theta) = \begin{pmatrix} C\theta & 0 & S\theta & 0 \\ 0 & 1 & 0 & 0 \\ -S\theta & 0 & C\theta & 0 \\ 0 & 0 & 0 & 1 \end{pmatrix} \quad (2.5)$$

$${}^A T_B = Rot(z, \theta) = \begin{pmatrix} C\theta & -S\theta & 0 & 0 \\ S\theta & C\theta & 0 & 0 \\ 0 & 0 & 1 & 0 \\ 0 & 0 & 0 & 1 \end{pmatrix}. \quad (2.6)$$

Properties of homogeneous transformation matrices

In this section some particular properties of homogeneous transformation matrix will be mentioned. The homogeneous transformation matrix can be divided as:

$${}^A T_B = \begin{pmatrix} s_x & n_x & a_x & P_x \\ s_y & n_y & a_y & P_y \\ s_z & n_z & a_z & P_z \\ 0 & 0 & 0 & 1 \end{pmatrix} = \begin{pmatrix} R & P \\ 0 & 0 & 0 & 1 \end{pmatrix}, \quad (2.7)$$

where R is the rotational matrix and column vector P represents the translation.

- Matrix R is orthogonal. That means the inverse of R is equal to its transpose.
- The inverse of ${}^A T_B$ is equal to ${}^B T_A$.
- If a frame R_0 undergoes k consecutive transformations and if each of them i , ($i = 0, \dots, k$) is determined in the current frame R_{i-1} then the transformation ${}^0 T_k$ will be the following multiplication:

$${}^0 T_k = {}^0 T_1 {}^1 T_2 {}^2 T_3 \dots {}^{k-1} T_k. \quad (2.8)$$

- Let ${}^A T_B$ is the transformation from frame $\{A\}$ to frame $\{B\}$. If the frame $\{B\}$ is subjected to a transformation T which is determined in the frame $\{A\}$ then the frame $\{B\}$ will be changed to $\{B'\}$ with

$${}^A T_{B'} = T {}^A T_B. \quad (2.9)$$

The above properties will be exploited in the next chapters especially in the chapters regarding transformations operation.

2.1.2. Kinematic screw [14]

Definition of a screw

Suppose that we have a vector field V on \mathbb{R}^3 . It is called a screw if there is a point O_A and a vector Ω and the following relation holds for every point O_B in R^3 :

$$V_B = V_A + \Omega \times O_A O_B, \quad (2.10)$$

where V_B is the vector of V at O_B and Ω is called the screw of V . For a pair of points O_X and O_Y we can easily deduce that

$$V_Y = V_X + \Omega \times O_X O_Y. \quad (2.11)$$

Therefore, the vectors V_A and Ω determine a screw at an arbitrary point O_A , which can be combined into a single vector (6×1)

$$\begin{pmatrix} V_A \\ \Omega \end{pmatrix}.$$

We can see that a vector field of velocity of a rigid body has above characteristics and thus it defines a so-called *kinematic screw*. For every point O_A on the rigid body, the kinematic screw at this point is composed of 2 parts. They are translational velocity V_A and angular velocity ω which are defined relatively in a fixed frame $\{R_0\}$.

Transformation of screws

Suppose that kinematic screw in O_A , origin of frame $\{A\}$, expressed in frame $\{A\}$ is described as ${}^A V_A$ and ${}^A \omega_A$. In order to compute the kinematic screw in O_B , ${}^B V_B$ and ${}^B \omega_B$ in frame B we have the following relation:

$$\begin{cases} \omega_B = \omega_A \\ V_B = V_A + \omega_A \times L_{A,B} \end{cases}, \quad (2.12)$$

with $L_{A,B}$ is the vector from O_A to O_B . Therefore, we have following relation:

$$\begin{pmatrix} V_B \\ \omega_B \end{pmatrix} = \begin{pmatrix} I_3 & -L_{A,B} \\ O_3 & I_3 \end{pmatrix} \begin{pmatrix} V_A \\ \omega_A \end{pmatrix}, \quad (2.13)$$

where I_3 and O_3 are the (3×3) identity matrix and zero matrix respectively. Projecting this relation onto frame A , we achieve:

$$\begin{pmatrix} {}^A V_B \\ {}^A \omega_B \end{pmatrix} = \begin{pmatrix} I_3 & -{}^A P_B \\ O_3 & I_3 \end{pmatrix} \begin{pmatrix} {}^A V_A \\ {}^A \omega_A \end{pmatrix}, \quad (2.14)$$

Because ${}^B V_B = {}^B R_A {}^A V_B$ and ${}^B \omega_B = {}^B R_A {}^A \omega_B$ multiplying 2 sides of Eq. (2.14) with ${}^B R_A$ we deduce that:

$$\begin{pmatrix} {}^B V_B \\ {}^B \omega_B \end{pmatrix} = \begin{pmatrix} {}^B R_A & -{}^B R_A {}^A P_B \\ O_3 & {}^B R_A \end{pmatrix} \begin{pmatrix} {}^A V_A \\ {}^A \omega_A \end{pmatrix}. \quad (2.15)$$

From above relation the screw transformation from frame $\{B\}$ to the frame $\{A\}$ is as follows:

$${}^B \mathbb{T}_A = \begin{pmatrix} {}^B R_A & -{}^B R_A {}^A P_B \\ O_3 & {}^B R_A \end{pmatrix}, \quad (2.16)$$

Representation of forces

The combination of forces and moments acting on a body at a point O_A can be reduced to a wrench $\begin{pmatrix} f_A \\ m_A \end{pmatrix}$ which is composed of a force f_A and a moment m_A . We can see that the vector field of moment is a screw where f_A is the screw of the field. Therefore, the wrench characterizes a screw. We note that

$$\begin{pmatrix} {}^B m_B \\ {}^B f_B \end{pmatrix} = {}^B \mathbb{T}_A \begin{pmatrix} {}^A m_A \\ {}^A f_A \end{pmatrix}, \quad (2.17)$$

where ${}^B \mathbb{T}_A$ is the screw transformation (6×6) from the frame $\{B\}$ to the frame $\{A\}$ defined as Eq. (2.16). From that we have

$$\begin{cases} {}^B f_B = {}^B R_A {}^A f_A \\ {}^B m_B = {}^B R_A ({}^A f_A \times {}^A P_B + {}^A m_A) \end{cases}. \quad (2.18)$$

And finally we obtain a more practical formula:

$$\begin{pmatrix} {}^B f_B \\ {}^B m_B \end{pmatrix} = \begin{pmatrix} {}^B R_A & 0 \\ {}^B R_A \times {}^B P_A & {}^B R_A \end{pmatrix} \begin{pmatrix} {}^A f_A \\ {}^A m_A \end{pmatrix}. \quad (2.19)$$

This transformation will be utilized for force and torque calculation of force feedback in the chapter tele-operation.

2.2. Cartesian impedance controller

In this section the general Cartesian impedance controller will be described since this controller will be exploited in the chapter teleoperation for design of the slave controller and in chapter stiffness identification to produce the unstable force field.

2.2.1. Impedance controller concept

By measuring human arm impedance Neville Hogan in [22] has proposed the hypothesis that the human central nervous system controls the movement by generating the virtual desired trajectory and modulating the impedance of the arm in order to produce motion. This idea has been realized as Cartesian impedance controller which has shown certain advantages. Instead of commanding force or position directly the controller commands indirectly force and torque through the desired impedance, the desired motion and current position of the robot. By tuning impedance parameters including stiffness damping and inertia the controller can generate variable dynamics of the end effector as illustrated in Fig. 2.1. In this fashion, when interacting with the surrounding environment the controller can modulate different impedance parameters that satisfy requirements of interaction.

In the book [29], the model describing the motion of the robot is given by:

$$M(q)\ddot{q} + C(q, \dot{q})\dot{q} + g(q) = \tau + \tau_{ext}, \quad (2.20)$$

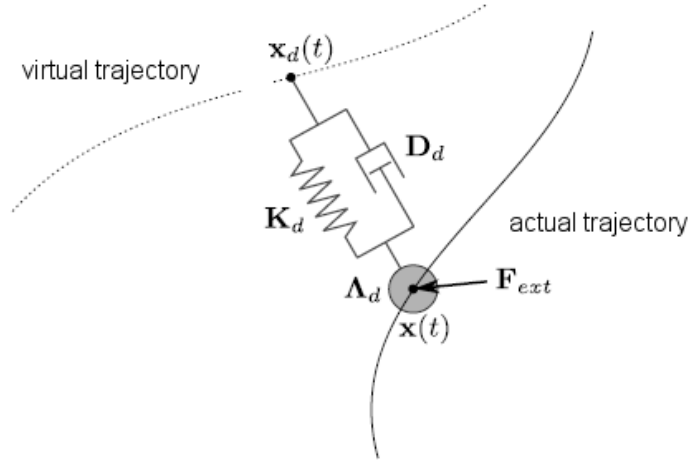


Figure 2.1.: The impedance controller principle [26]

where $M(q)$ is the mass matrix which is symmetric, $C(q, \dot{q})$ is Coriolis and centrifugal matrix, $g(q)$ is vector of gravitation and τ and τ_{ext} are the joint torque and external torque respectively.

The objective of the Cartesian impedance controller is to obtain the external force that holds the following dynamical behaviour:

$$\Lambda_d \ddot{\tilde{x}} + D_d \dot{\tilde{x}} + K_d \tilde{x} = F_{ext}, \quad (2.21)$$

where $\tilde{x} = x - x_d \in \mathbb{R}^m$ the difference between the current position x and the desired position x_d of the robot end effector. Λ_d , D_d and K_d are the symmetric and positive defined matrices of desired inertia, damping and stiffness. In order to realize the controller an interpolator is required which will generate the desired trajectory that the end effector of the robot will follow. For example, the interpolator with minimum jerk trajectory can be utilized.

The relation between task coordinate and joint coordinate is given by $x = f(q)$. With definition of Jacobian $J(q) = \partial f(q) / \partial q$ we obtain the relation between the velocity in task coordinate and joint velocity as follows:

$$\dot{x} = J(q) \dot{q}, \quad (2.22)$$

And applying derivative over time on 2 sides of the equation Eq. (2.22) the acceleration in task coordinate depends on joint velocity and joint acceleration as:

$$\ddot{x} = \dot{J}(q) \dot{q} + J(q) \ddot{q}. \quad (2.23)$$

By assuming that Jacobian matrix is invertible we have

$$\dot{q} = J(q)^{-1} \dot{x}, \quad (2.24)$$

and

$$\ddot{q} = J(q)^{-1} \ddot{x} - J(q)^{-1} \dot{J}(q) \dot{q}. \quad (2.25)$$

2. Theoretical background

Substituting Eq. (2.24) and Eq. (2.25) into equation Eq. (2.20) we achieve the following equation

$$\Lambda(q)\ddot{x} + \mu(q, \dot{q})\dot{x} + J(q)^{-T}g(q) = J(q)^{-T}\tau + F_{ext}, \quad (2.26)$$

with Cartesian inertia matrix

$$\Lambda(q) = J(q)^{-T}M(q)J(q)^{-1},$$

and Cartesian Coriolis and centrifugal matrix

$$\mu(q, \dot{q}) = J(q)^{-T} \left(C(q, \dot{q}) - M(q)J(q)^{-1}\dot{J}(q) \right) J(q)^{-1}.$$

Substituting equation Eq. (2.21) into Eq. (2.26) the control input F_τ is as follows:

$$F_\tau = J(q)^{-T}\tau = F_g(x) + \Lambda(q)\ddot{x}_d + \mu(q, \dot{q})\dot{x} - \Lambda(q)\Lambda_d^{-1}(K_d\tilde{x} + D_d\dot{\tilde{x}}) + (\Lambda(q)\Lambda_d^{-1} - I)F_{ext}. \quad (2.27)$$

But the joint torque is actually applied to control the robot. Therefore, the control input is given by

$$\begin{aligned} \tau = J(q)^T F_\tau = & g(q) + J(q)^T(\Lambda(q)\ddot{x}_d + \mu(q, \dot{q})\dot{x}) - \\ & J(q)^T \Lambda(q)\Lambda_d^{-1}(D_d\dot{\tilde{x}} + K_d\tilde{x})J(q)^T(\Lambda(q)\Lambda_d^{-1} - I)F_{ext}. \end{aligned} \quad (2.28)$$

By choosing the desired inertia Λ_d equal to $\Lambda(q)$ we can avoid the force feedback term F_{ext} that leads to the following control law:

$$\tau = g(q) + J(q)^T(\Lambda(q)\ddot{x}_d + \mu(q, \dot{q})\dot{x} - D_d\dot{\tilde{x}} - K_d\tilde{x}). \quad (2.29)$$

Looking at the control law we can see that it is composed of two important components. The first one is the gravity compensation which purely support the robot against the gravitational force. The second term is for modulating the impedance force which is composed of three elements that are the inertia force $\Lambda(q)\ddot{x}_d$, the damping force $D_d\dot{\tilde{x}}$ and the elastic force $K_d\tilde{x}$. In practice, the Coriolis force $\mu(q, \dot{q})\dot{x}$ can be ignored to reduce computation because of its small effect in the controller. One problem arises is the occurrence of kinematic singularity. This issue will be treated in the next section.

2.2.2. Kinematic singularity avoidance

The idea of kinematic singularity avoidance is that we define a measure of singularity. When this quantity reaches a certain threshold the robot is controlled orthogonally to the direction of singularity that drives the robot away from the singular position [29]. The measure of singularity is a function of Jacobian matrix:

$$m_{kin}(q) = \sqrt{\det(J(q)J^T(q))}. \quad (2.30)$$

Looking at this definition of kinematic singularity measure we can see that when kinematic singularity occurs, i.e $\det J(q) = 0$, the measure of singularity is equal to zero. In order

to generate the force that drive the robot orthogonally to the direction of singularity a singularity avoidance potential is defined as follows:

$$Vm(q) = \begin{cases} ks(m_{kin}(q) - m_0)^2 & m_{kin} \leq m_0 \\ 0 & m_{kin} > m_0 \end{cases} . \quad (2.31)$$

The equation shows that when the robot approaches the defined area of singularity the potential of the force field is activated. Therefore, the overall torque that controls the robot is composed of the one of Cartesian impedance controller and the one caused by this potential:

$$\begin{aligned} \tau &= \tau_c - \partial Vm(q)/\partial q \\ &= \tau_c - \left(1 - \frac{m_0}{m_{kin}(q)}\right) \frac{\partial f(q)}{\partial q} , \end{aligned} \quad (2.32)$$

where τ_c is the output from Cartesian impedance controller and $f(q)$ is equal to $\det(J(q)J^T(q))$.

3. Human Arm Identification

3.1. Geometrics Identification

3.1.1. The direct geometric model

The geometrics of human arm is modelled by two rigid bodies (the upper arm and the forearm) with five degree of freedoms (three in the shoulder and two in the elbow). The form of a rigid body system is considered to be invariant during movement [15] with following properties:

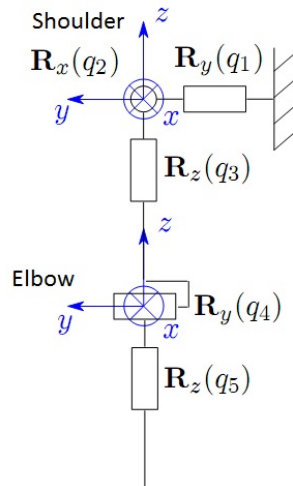


Figure 3.1.: The human arm model [27]

- The segments are rigid bodies which have invariant form.
- The shoulder joint is a spherical joint which has the center of rotation not moving relatively to the scapula bone and the upper arm.
- The elbow joint is a skew-oblique joint, the flexion-extension axis is not moving relatively to the humerus bone, the pronation-supination axis is not moving relatively to the forearm.

In Fig. 3.1 the direct geometric model [27] with three degrees of freedom in the shoulder can be attributed to anteversion-retroversion $R_y(q_1)$, abduction-adduction $R_x(q_2)$, and external-internal rotation $R_z(q_3)$ of the humerus relative to the scapula and two degrees of freedom in the elbow joint corresponding to flexion-extension rotation $R_y(q_4)$ and pronation-supination rotation $R_z(q_5)$.

The direct geometric model defines the location of endpoint as a function of joint coordinates, $x = f(q)$.

$$T(q) = R_y(q_1)R_x(q_2)R_z(q_3)D_z(a)R_y(q_4)R_z(q_5)D_x(d_x)D_y(d_y)D_z(d_z) \quad (3.1)$$

The direct geometric model depends on the geometric parameters a and $d = [d_x d_y d_z]^T$ of the human arm. In order to estimate those geometric parameters, the joint positions must be identified.

Identification of joint position

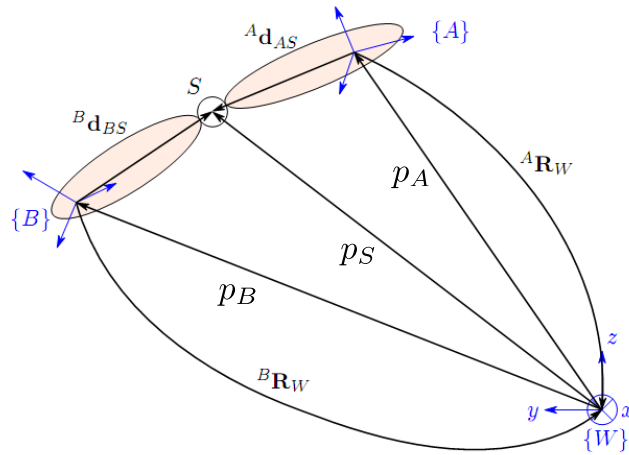


Figure 3.2.: The joint identification approach [27]



Figure 3.3.: The placement of marker sets

In this section the joint position identification method in [27] and [15] will be utilized. To identify the joint position between two links two marker sets must be placed on each link like in Fig. 3.2 and Fig. 3.3. Each marker set has its own coordinate. The positions and orientation of these two marker sets will be tracked by *Vicon Motion Capture system*. The position of the joint will be calculated with the following formulas:

$$p_{S'} = p_A + {}^A R_W^T A d_{AS} , \quad (3.2)$$

3. Human Arm Identification

$$p_{S''} = p_B + {}^B R_W^T {}^B d_{BS}, \quad (3.3)$$

where p_A and $p_B \in \mathbb{R}^{3 \times 1}$ are the position vectors from the origin of the world coordinate $\{W\}$ to the origins of marker coordinates $\{A\}$ and $\{B\}$ expressed in the world coordinate $\{W\}$. ${}^A R_W$ and ${}^B R_W \in \mathbb{R}^{3 \times 3}$ are the rotation matrices of the transformation from coordinate $\{A\}$ and $\{B\}$ to the world coordinate $\{W\}$. ${}^A d_{AS}$ and ${}^B d_{BS}$ are the vectors from origins of coordinate $\{A\}$ and $\{B\}$ to the joint position S in the marker coordinate $\{A\}$ and $\{B\}$ respectively. Due to the assumption of rigid bodies, those vector are not varying. ${}^A d_{AS}$ and ${}^B d_{BS}$ are determined in such a way that the integral of the quadratic error

$$\Delta p_S = \frac{1}{N} \int_0^N \underbrace{[(p_{S'} - p_{S''})^T (p_{S'} - p_{S''})]}_{f({}^A d_{AS}, {}^B d_{BS})} dk \quad (3.4)$$

will be minimized. Where N is the number of the discrete time k . Substituting Eq. (3.2) and Eq. (3.3) in Eq. (3.8) results in the cost function depending on the ${}^A d_{AS}$ and ${}^B d_{BS}$ as follows:

$$\begin{aligned} f({}^A d_{AS}, {}^B d_{BS}) = & p_A^T p_A + p_A^{TW} R_A {}^A d_{AS} - p_A^T p_B - p_A^{TW} R_B {}^B d_{BS} \\ & + {}^A d_{AS}^T {}^A R_W p_A + {}^A d_{AS}^T {}^A d_{AS} - {}^A d_{AS}^T {}^A R_W p_B \\ & - {}^A d_{AS}^T {}^A R_W {}^W R_B {}^B d_{BS} - p_B^T p_A - p_B^{TW} R_A {}^A d_{AS} + p_B^T p_B \\ & + p_B^{TW} R_B {}^B d_{BS} - {}^B d_{BS}^T {}^B R_W p_A - {}^B d_{BS}^T {}^B R_W {}^A R_W^T {}^A d_{AS} \\ & + {}^B d_{BS}^T {}^B R_W p_B + {}^B d_{BS}^T {}^B d_{BS}. \end{aligned} \quad (3.5)$$

Through partial derivative of $f({}^A d_{AS}, {}^B d_{BS})$ with respect to ${}^A d_{AS}$ and ${}^B d_{BS}$ we obtain the gradient:

$$\frac{\partial f({}^A d_{AS}, {}^B d_{BS})}{\partial {}^A d_{AS}^T} = 2 {}^A R_W p_A + 2 E_3 {}^A d_{AS} - 2 {}^A R_W p_B - 2 {}^A R_W {}^W R_B {}^B d_{BS} \quad (3.6)$$

$$\frac{\partial f({}^A d_{AS}, {}^B d_{BS})}{\partial {}^B d_{BS}^T} = 2 {}^B R_W p_B + 2 E_3 {}^B d_{BS} - 2 {}^B R_W p_A - 2 {}^B R_W {}^W R_A {}^A d_{AS} \quad (3.7)$$

Setting the gradient to zero and rearranging the terms in matrix notation and integrating it over time there will be a linear equation:

$$\int_0^N D dk \cdot z = \int_0^N b dk, \quad (3.8)$$

where $D \in \mathbb{R}^{6 \times 6}$ and $z, b \in \mathbb{R}^{6 \times 1}$ as following:

$$\begin{aligned} D &= \begin{pmatrix} E_3 & -{}^A R_W {}^W R_B \\ -{}^B R_W {}^A R_W^T & E_3 \end{pmatrix}, \\ z &= \begin{pmatrix} {}^A d_{AS} \\ {}^B d_{BS} \end{pmatrix}, \\ b &= \begin{pmatrix} {}^A R_W (p_B - p_A) \\ {}^B R_W (p_A - p_B) \end{pmatrix}. \end{aligned}$$

Solving the Eq. (3.8) we obtain the joint positions ${}^A d_{AS}$ and ${}^B d_{BS}$ with respect to the markers coordinates $\{A\}$ and $\{B\}$, where the quadratic mean value Δp_S is minimized.

$$z = \begin{pmatrix} {}^A R_W(p_B - p_A) \\ {}^B R_W(p_A - p_B) \end{pmatrix} = \left(\int_0^N Ddk \right)^{-1} \left(\int_0^N bdk \right) \quad (3.9)$$

The method is applied only for two cutting axes. In the case of human arm, we need three marker $\{1\}$, $\{2\}$ and $\{3\}$ as shown in Fig. 3.4. Marker set $\{1\}$ is placed somewhere near the shoulder, marker sets $\{2\}$ and $\{3\}$ are placed on upper arm and forearm respectively. The position of shoulder joint is calculated through ${}^1 d_{1S}$ and ${}^2 d_{2S}$ and the position of elbow is computed through ${}^2 d_{2E}$ and ${}^2 d_{3E}$.

Constant parameters

Through the positions of shoulder joint in the marker coordinate $\{2\}$ ${}^2 d_{2S}$ and the rotation matrix of the marker coordinate $\{2\}$ in the world coordinate $\{W\}$, R_W^T the homogeneous transformation matrix from the world to the shoulder coordinate will be computed as follows:

$${}^W T_S = \begin{pmatrix} E_3 & p_2 + {}^W R_2 {}^2 d_{2S} \\ 0 & 1 \end{pmatrix} \quad (3.10)$$

Therefore the position of the shoulder is known. It is noticed that when the geometrics is identified the subject has to sit in the way that the rotation matrix of the shoulder coordinate in the world coordinate equals the identity matrix. Otherwise the above calculation will be wrong.

The length of the upper arm a can be obtained by using Euclidean norm of the sum vector of ${}^2 d_{2S}$ and ${}^2 d_{2E}$

$$a = \left\| -{}^2 d_{2S} + {}^2 d_{2E} \right\|_2 . \quad (3.11)$$

The coordinate of the forearm $\{U\}$ is located at the marker coordinate $\{3\}$. The z_U is identical with the rotational axis q_5 , the positive direction points to the shoulder. y_U has the same direction of y_S at the resting position shown in Fig. 3.1, and x_U defines the full coordinate. The transformation matrix ${}^3 T_U$ from marker coordinate $\{3\}$ to $\{U\}$ is determined as follows:

$${}^3 T_U = \begin{pmatrix} {}^U R_3^T & 0 \\ 0 & 1 \end{pmatrix} , \quad (3.12)$$

where the rotation matrix ${}^U R_3$ depends on the way of placing marker set $\{3\}$. In the experiment it is given as:

$${}^3 R_U = \begin{pmatrix} 0 & 0 & -1 \\ -1 & 0 & 0 \\ 0 & 1 & 0 \end{pmatrix}$$

The vector d from the elbow to the marker set 3 expressed in the $\{U\}$ coordinate is computed as:

$$d = {}^U d_{3E} = {}^U R_3 {}^3 d_{3E} , \quad (3.13)$$

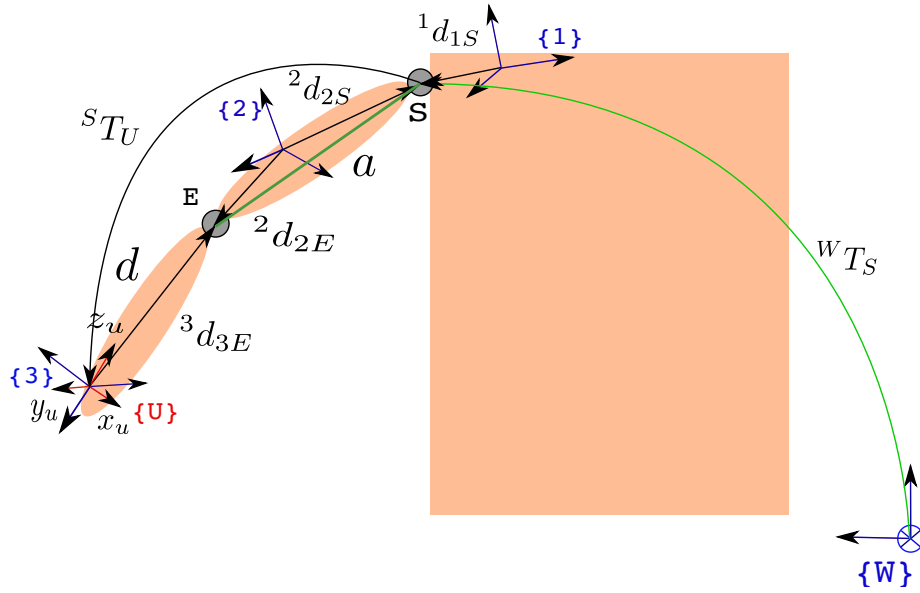


Figure 3.4.: The geometric parameters and the transformations in geometric identification [27]

with constant parameters d and a from Eq. (3.11) and Eq. (3.13) the direct geometrics of the arm $T(q)$ defined from Eq.(3.1) for each point of time k can be calculated as a function of q . On the other hand, we can see that, the direct geometrics of the human arm ${}^S T_U$ can be computed through the measured position of marker set 3, ${}^W T_3$ from the camera system as follows:

$${}^S T_U = {}^W T_S^T {}^W T_3 {}^U T_3^T \quad (3.14)$$

This value will be used as the desired transformation $T(d)$ of $T(q)$ in the Eq. (3.1) and will be utilized in inverse geometric model.

3.1.2. The inverse geometric model [27]

The inverse geometric model is the mapping from Cartesian coordinates to the joint coordinates:

$$q = f^{-1}(x)$$

In order to calculate inverse geometrics of human arm, the same optimization method described in [27] is exploited. The joint coordinates are calculated by means of minimizing the model error which is defined by a cost function:

$$\operatorname{argmin}(f(q)),$$

where the cost function $f(q)$ which measures the difference between the desired transformation matrix and the direct geometrics is a Frobenius norm

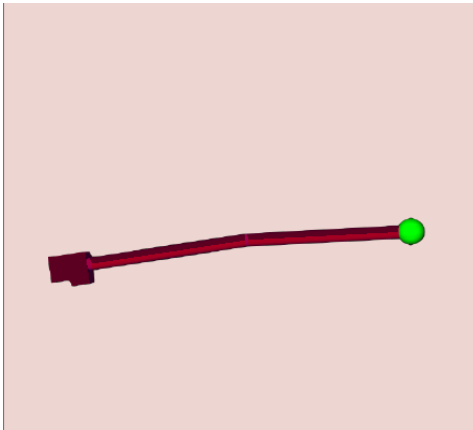
$$f(q) = \|T(q)T_d^{-1} - E_4\|_F, \quad (3.15)$$

where T_d is the transformation matrix of the U coordinate to the shoulder coordinate which is computed as Eq. (3.14) and the $T(q)$ is the direct geometrics calculated according to the Eq. (3.1).

That is a non-linear and unconstrained optimization problem which can be solved by a function *fminunc* in MATLAB *Optimization Toolbox*. The gradient of the cost function is given to reduce the computation time of the algorithm. In this way the inverse geometrics can be computed on-line when the initial values and the geometric information, including the length of the upper arm a and force arm d are provided. The local optimum is unavoidable especially when the arm configuration is at singular positions. However in other cases the result was good enough.

3.1.3. Experiment setup and result

The star markers are placed on the subject arm as can be seen in Fig. (3.5) and the subject moves his arm in the space according to the virtual arm movement in the simulation environment through a predefined set of configurations shown in Table 3.1 and 3.2.



(a) The virtual arm



(b) The human arm movement

Figure 3.5.: Geometrics identification setup

Table 3.1.: The start predefined arm configurations

Configurations	$q_1(rad)$	$q_2(rad)$	$q_3(rad)$	$q_4(rad)$	$q_5(rad)$
Q_{start1}	0	0	0	0	0
Q_{start2}	0	0	0	0	0
Q_{start3}	0	0	0	pi/2	0
Q_{start4}	0	0	0	pi/2	0
Q_{start5}	0	0	0	pi/2	0

3. Human Arm Identification

Table 3.2.: The final predefined arm configurations

Configurations	$q_1(rad)$	$q_2(rad)$	$q_3(rad)$	$q_4(rad)$	$q_5(rad)$
Q_{final1}	pi/2	0	0	0	0
Q_{final1}	0	pi/2	0	0	0
Q_{final1}	0	0	pi/4	pi/2	0
Q_{final1}	0	0	0	0	0
Q_{final1}	0	0	0	pi/2	pi/4

Table 3.3.: Joint position identification result

	${}^1d_{1S}$	${}^2d_{2S}$	${}^2d_{2E}$	${}^3d_{3E}$
x (m)	-0.078	-0.219	0.067	-0.198
y (m)	-0.554	0.048	-0.021	0.0175
z (m)	0.662	-0.039	-0.026	-0.024

From the result of joint identification in Table 3.3 the constant parameters a and d can be computed as Eq. (3.11) and (3.13) with $a = 0.295m$ and $d = [d_x \ d_y \ d_z] = [-0.018m \ -0.024m \ 0.198m]$

The geometric identification of human arm is quite precise with high repeatability of constant parameters a and d when the subject moves his arm correctly. However during the arm movement if the subject moves his shoulder or skin where the makers are placed moves relatively to the arm then the error will be increased. Another possible error comes from the Vicon camera system when it cannot recognize all the markers at some point of arm movement or recognize the marker coordinates wrongly. In order to avoid this error the camera system must be calibrated precisely and the working range of each camera should cover the movement of the arm during identification phase. The time for this task lasts approximately 5 minutes.

3.2. Inertial parameter identification

Inertial parameters of human arm are very important for investigation of *human arm dynamics*. However until now in addition to physiological methods, there is no reliable *non-invasive* method to do that. In the past, some methods have been considered like using measurement of human arm volume and using some statistic data from physiology, or using the human arm dynamics model with assumption that human arm and body are the system of rigid body. However that assumption is violated because each joint of human arm is a flexible joint and the body itself is not rigid enough. That causes the force and torque under the chair when the subject moves his arm not exactly match the dynamics. In this work a simple method will be proposed to identify all those standard inertial parameters which are used for describing the human arm dynamics.

3.2.1. Formulation of the method

Modelling of the arm inertial parameter

The human arm includes two parts, the upper arm and lower arm. We assume that each part of the arm has geometry like a cylinder with the length, diameter and the symmetric density distribution as depicted in Fig. 3.6. According to this assumption, we can have following inertial parameters of each link:

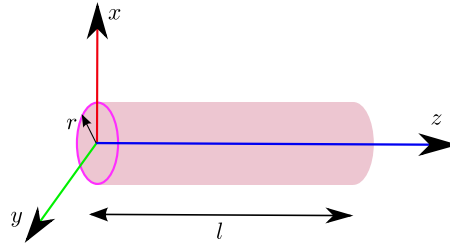


Figure 3.6.: Link model

1. The mass of the link: m
2. The mass moment: $m_x = m_y = 0, m_z$
3. The moment of inertia: $I_x = I_y, I_z, I_{xy} = I_{xz} = I_{yz} = 0$

The inertia matrix:
$$\begin{bmatrix} ml^2/3 & 0 & 0 \\ 0 & ml^2/3 & 0 \\ 0 & 0 & mr^2/2 \end{bmatrix}$$

From this model we only need to identify four inertial parameters for each link of the human arm. Those parameters have the main contribution to the dynamics of the human arm.

Mathematical formulation

When the subject sits on the chair like in Fig. 3.8 and 3.10 we consider the arm and the body as three serial links system and we can use the backward Newton- Euler computation [14] to calculate the force and the torque acting on each joint and the sensor under the chair in the static case.

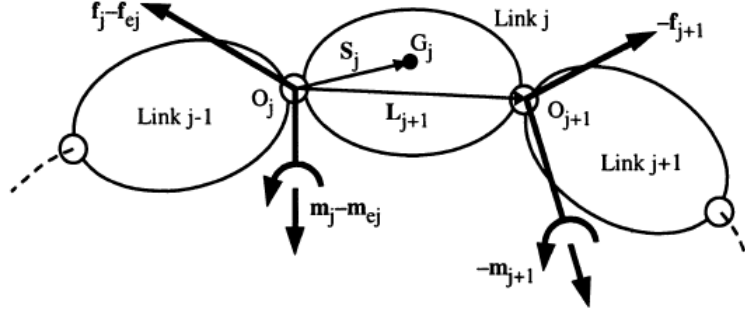


Figure 3.7.: Forces and moments on link j [14]

we consider a link j with the origin O_j of its frame R_j is located on its joint axis. External force on link j , \mathbf{F}_j , and moment of external forces on link j about O_j , \mathbf{M}_j , are given as follows:

$$\begin{cases} \mathbf{F}_j = \mathbf{f}_j - \mathbf{f}_{j+1} + M_j \mathbf{g} - \mathbf{f}_{ej} \\ \mathbf{M}_j = \mathbf{m}_j - \mathbf{m}_{j+1} - \mathbf{L}_{j+1} \times \mathbf{f}_{j+1} + \mathbf{S}_j \times M_j \mathbf{g} - \mathbf{m}_{ej} \end{cases} \quad (3.16)$$

where \mathbf{f}_j is the force exerted on link j by link $j - 1$; M_j is the mass of link j ; \mathbf{g} is the vector of gravitational acceleration; \mathbf{m}_j is the moment about O_j exerted on link j by link $j - 1$; \mathbf{L}_{j+1} is the position vector from O_j to O_{j+1} ; \mathbf{S}_j is the vector $O_j G_j$ from O_j to the center of mass of the link, G_j ; \mathbf{m}_{ej} and \mathbf{f}_{ej} are the moment about O_j and the force exerted by link j on environment. In our consideration, there is no force or moment exerted by link j on the environment. Therefore, both \mathbf{m}_{ej} and \mathbf{f}_{ej} are equal to zero. In the stationary case and we have $\mathbf{F}_j = 0$ and $\mathbf{M}_j = 0$. Hence, from Eq. (3.16) we deduce that

$$\begin{cases} \mathbf{f}_j = \mathbf{f}_{j+1} - M_j \mathbf{g} \\ \mathbf{m}_j = \mathbf{m}_{j+1} + \mathbf{L}_{j+1} \times \mathbf{f}_{j+1} - \mathbf{S}_j \times M_j \mathbf{g} \end{cases} \quad (3.17)$$

Applying this calculation we can compute recursively backward the wrench acts the elbow joint, the shoulder joint and the last joint located at the sensor frame by initializing $\mathbf{f}_4 = 0$ and $\mathbf{m}_4 = 0$.

The force and torque act on the elbow joint:

$$\begin{cases} \mathbf{f}_3 = -M_3 \mathbf{g} \\ \mathbf{m}_3 = -\mathbf{S}_3 \times M_3 \mathbf{g} \end{cases} \quad (3.18)$$

where M_3 is the mass of the forearm. The force and torque act on the shoulder joint:

$$\begin{cases} \mathbf{f}_2 = \mathbf{f}_3 - M_2 \mathbf{g} = -(M_2 + M_3) \mathbf{g} \\ \mathbf{m}_2 = \mathbf{m}_3 + \mathbf{L}_3 \times \mathbf{f}_3 - \mathbf{S}_2 \times M_2 \mathbf{g} = -\mathbf{S}_3 \times M_3 \mathbf{g} - \mathbf{L}_3 \times M_3 \mathbf{g} - \mathbf{S}_2 \times M_2 \mathbf{g} \end{cases} \quad (3.19)$$

where the M_2 is the mass of the upper arm. The force and torque act on the sensor under the chair:

$$\begin{cases} \mathbf{f}_1 = \mathbf{f}_2 - M_1 \mathbf{g} = -(M_1 + M_2 + M_3) \mathbf{g} \\ \mathbf{m}_1 = -\mathbf{S}_3 \times M_3 \mathbf{g} - \mathbf{L}_3 \times M_3 \mathbf{g} - \mathbf{S}_2 \times M_2 \mathbf{g} - \mathbf{L}_2 \times (M_2 + M_3) \mathbf{g} + \mathbf{S}_1 \times M_1 \mathbf{g} \end{cases} \quad (3.20)$$

where M_1 is the mass of the rest of the human body. Finally, the wrench at the sensor is as following:

$$\begin{cases} \mathbf{f} = -(M_1 + M_2 + M_3)\mathbf{g} \\ \mathbf{m} = -(\mathbf{L}_2 + \mathbf{L}_3 + \mathbf{S}_3) \times M_3\mathbf{g} - (\mathbf{L}_2 + \mathbf{S}_2) \times M_2\mathbf{g} - \mathbf{S}_1 \times M_1\mathbf{g} \end{cases} \quad (3.21)$$

Looking at the relation of the wrench with the mass of upper arm and the lower arm and their center of mass, by changing the configuration of the arm to predefined positions we can calculate $S_3 \times M_3g$ and $S_2 \times M_2g$, where S_3 is the length of vector \mathbf{S}_3 and S_2 is the length of vector \mathbf{S}_2 . If we know S_3 and S_2 the mass of the forearm and upper arm can be calculated. From those values the other inertial parameters can be calculated.

3.2.2. Experiment setup and result

The subject sits on a chair in such a way that his shoulder and body is fixed relatively with the chair by using a belt and puts his arm at the different configurations defined in the table 3.4. The arm configuration will be tracked by the camera system. When the subject

Table 3.4.: The arm configurations for inertial parameter identification

Configurations	$q_1(rad)$	$q_2(rad)$	$q_3(rad)$	$q_4(rad)$	$q_5(rad)$
1	0	pi/2	0	0	0
2	0	pi/2	0	pi/2	0
3	pi/2	0	0	0	pi/2

puts his arm correctly the recording of the torque under the chair will start.



(a) Configuration 1

(b) Configuration 2

Figure 3.8.: Configurations 1 and 2

3. Human Arm Identification

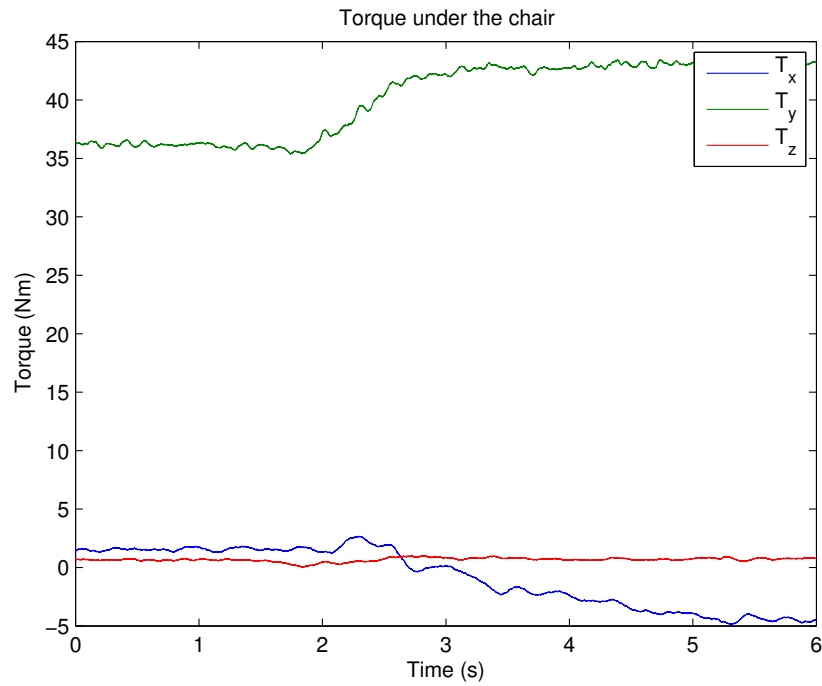


Figure 3.9.: Changes of torque when the subject is moving his arm from configuration 1 to 2

The difference of the moment about the x axis on the sensor is : $S_3 \times M_3g$.

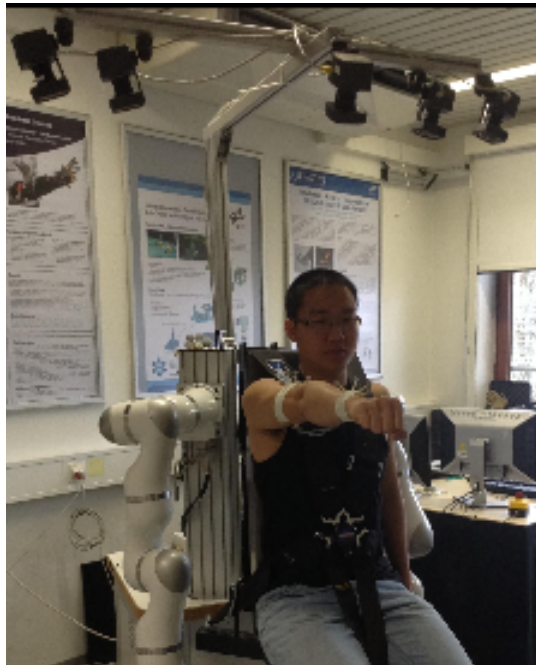


Figure 3.10.: Configuration 3

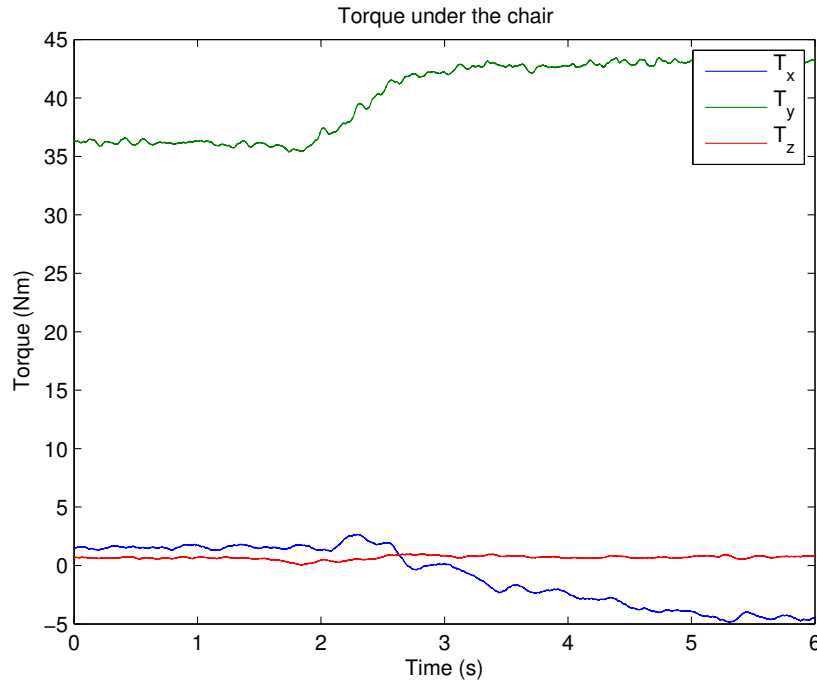


Figure 3.11.: Changes of torque when the subject is moving his arm from configuration 1 to 3

For configurations 1 and 2 as shown in Fig. 3.8 the changes of measured torque under the chair is illustrated in Fig. 3.9. The mean value of torque of 500 beginning samples and 500 samples at the end of the file will be extracted to calculate the changes of the torque.

Similarly, the subject moves his arm from configuration 1 to configuration 3 as can be seen in Fig. 3.8 and 3.10 and the changes in torque about the x axis is shown in Fig. 3.11. The difference of the moment about x axis on the sensor between configuration 1 and 3 is : $S_3 \times M_3g + L_3 \times M_3g + S_2 \times M_2g$ where L_3 is the length of vector \mathbf{S}_3 , the length of upper arm.

Table 3.5.: The measured inertial parameters

Inertial Parameters	The force arm	The upper arm
M (kg)	1.5278	1.6975
m_z (kgm)	0.2911	0.2731
I_x, I_y (kgm ²)	0.0553	0.0444
I_z (kgm ²)	0.00068	0.0014

Using geometric identification of the human arm we can have the length of the upper arm and the lower arm $L_3 = a = 0.295m$, $L_4 = d_z + \Delta z = 0.198 + 0.130 = 0.3280m$,

3. Human Arm Identification

where the Δz is the distance from the marker 3 to the end of the hand. Alternatively, we can measure those parameters directly without using a camera system. The radius of the upper arm and the lower arm will be directly measured $R_{ua} = 0.04m$, $R_{la} = 0.03m$. Using the data from physiological statistics [13] we can have $S_3 = \frac{57}{100}L_4$ and we assume that $S_2 = \frac{57}{100}L_3$. From that we can calculate the M_2 and M_3 and the remaining inertial parameters. Table 3.5 above shows the result of standard inertial parameters. We can see that the mass of lower arm and the upper arm are 1.53 kg and 1.70 kg. However the accuracy of the method highly depends on the posture of the subject when he moves his arm between different configurations. The subject should only move his arm correctly and keep the rest of the body the same for all configurations. And even the breath of the subject can change the measured torque significantly. Therefore the whole measurement should be done repeatedly 6 times to reduce the mentioned errors. It is noted that this method is only an approximation of human inertial parameters.

3.2.3. Mass matrix in Cartesian coordinate

The mass matrix is calculated as follows:

1. Calculate the mass matrix in the joint space $M(q)$.
2. Calculate the mass matrix in the Cartesian space $M_x(q) = J(q)^{-T}M(q)J(q)^{-1}$ with J is Jacobian matrix.

3.3. Stiffness identification

3.3.1. Human arm dynamic model in Cartesian coordinate

In this section the dynamic model of the human arm in Cartesian coordinate [26] will be described and analysed for endpoint stiffness identification. The Lagrange formulation of human arm motion in joint coordinate is given as follows:

$$M(q)\ddot{q} + C(q, \dot{q})\dot{q} + g(q) + h(q, \dot{q}) = \tau, \quad (3.22)$$

where $M(q)$ is the mass matrix, $C(q, \dot{q})$ is the Coriolis centrifugal matrix, $g(q)$ is the gravitation vector, $h(q, \dot{q})$ is the torque generated by the muscle, and τ is the external torque applied to the arm. The dynamic model of the human arm in Cartesian coordinates is given as

$$M_x(q)\ddot{x} + C_x(q, \dot{q})\dot{x} + g_x(q) + h_x(q, \dot{q}) = F, \quad (3.23)$$

where

$$\begin{aligned} M_x(q) &= J(q)^{-T}M(q)J(q)^{-1} \\ C_x(q, \dot{q}) &= J(q)^{-T}\left(C(q, \dot{q}) - M(q)J(q)^{-1}J(q)\right)J(q)^{-1} \\ g_x(q) &= J(q)^{-T}g(q) \\ h_x(q, \dot{q}) &= J(q)^{-T}h(q, \dot{q}), \end{aligned}$$

with $J(q)$ is the Jacobian matrix of the arm which relates the hand position with the joint coordinates q of the arm.

We assume a small displacement Δx of the hand around an equilibrium position x^* . we have:

$$x = x^* + \Delta x \quad (3.24)$$

$$\dot{x} = \dot{x}^* + \Delta \dot{x} \quad (3.25)$$

$$\ddot{x} = \ddot{x}^* + \Delta \ddot{x} = \Delta \ddot{x} \quad (3.26)$$

$$M_x(x) = M_x|_{x^*} + \frac{\partial M_x}{\partial x}|_{x^*} \Delta x \quad (3.27)$$

$$C_x(x, \dot{x}) = C_x|_{x^*} + \frac{\partial C_x}{\partial x}|_{x^*} \Delta x + \frac{\partial C_x}{\partial \dot{x}}|_{x^*} \Delta \dot{x} \quad (3.28)$$

$$g_x(x) = g_x|_{x^*} + \frac{\partial g_x}{\partial x}|_{x^*} \Delta x \quad (3.29)$$

$$h_x(x, \dot{x}) = h_x|_{x^*} + \frac{\partial h_x}{\partial x}|_{x^*} \Delta x + \frac{\partial h_x}{\partial \dot{x}}|_{x^*} \Delta \dot{x} \quad (3.30)$$

$$F = F^* + \Delta F \quad (3.31)$$

Substituting all above equations into the Eq. (3.23) and eliminating the very small terms containing $\Delta x \Delta \ddot{x}$, $\Delta x \Delta \dot{x}$ and $\Delta \dot{x} \Delta \dot{x}$ the local linearised dynamic model of human arm in Cartesian coordinate is as follows:

$$M_x \Delta \ddot{x} + D_x \Delta \dot{x} + K_x \Delta x = \Delta F \quad (3.32)$$

where

$$\begin{aligned} M_x &= M_x|_{x^*} \\ D_x &= C_x|_{x^*} + \frac{\partial h_x}{\partial \dot{x}}|_{x^*} \\ K_x &= \frac{\partial g_x}{\partial x}|_{x^*} + \frac{\partial h_x}{\partial x}|_{x^*} \end{aligned}$$

Looking at Equ. (3.32) we can see that the dynamics of the arm depends on Cartesian impedance which are Cartesian inertia M_x , Cartesian damping D_x and the Cartesian stiffness K_x . From this equation the static stiffness can be measured by perturbing position of the hand with a small displacement and measuring the static restoring forces before and after perturbation. This force is equal to the stiffness force because the inertial and the damping force in the static cases are zero. Therefore, the stiffness coefficient can be derived by dividing the force by the displacement.

3.3.2. The experiment setup

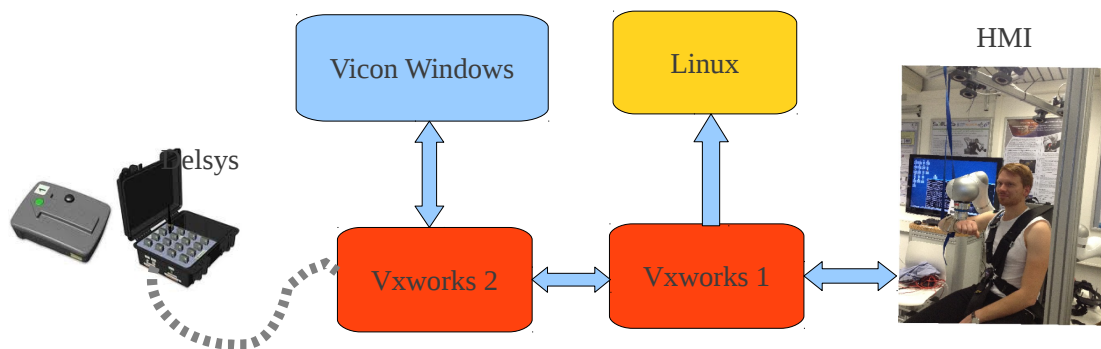


Figure 3.12.: The overview of the system

The whole system described in Fig. 3.12 consists of 2 real-time operating systems Vxworks. Vxworks 1 is used for controlling HMI hardware system including 2 lightweight robot arms while Vxworks 2 is used for collecting EMG data through *surface EMG sensors DelSys Trigno Wireless System*. In addition, this second real-time machine is connected with a windows operating system which is responsible for operating the Vicon camera system. A Linux operating system is used for monitoring and tuning parameters and visualizing the hand positions and perturbation information for subject participating in the experiment. A healthy subject is seated on a chair with a belt that helps to constrain the subjects shoulder position as shown in Fig. 3.18a. The subject's right elbow is supported by a rope attached to the ceiling that increases the ability of the arm to modulate the arm stiffness in the plane more flexibly and reduces the muscular fatigue during the experiment. The right forearm of the subject is inserted in a cuff that will be mounted on the end effector of a lightweight robot as can be seen in Fig. 3.1. The role of the cuff is to reduce the relative movement between the wrist and the connecting point due to the elasticity of the skin. The interaction force and moment between the hand will be recorded by a force torque sensor placed at the end effector of the robot.

Stiffness identification

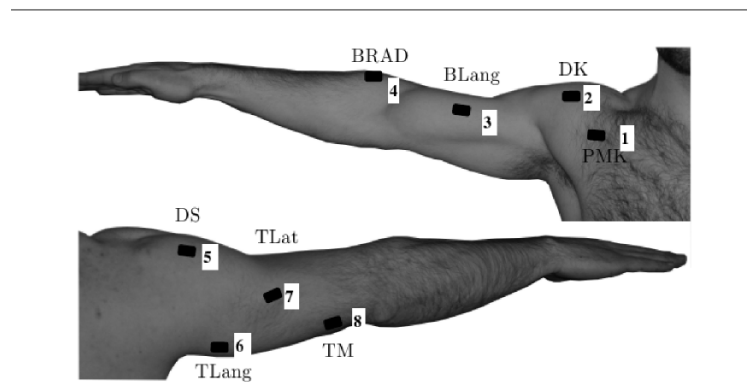


Figure 3.13.: EMG electrode placement [27]

Table 3.6.: EMG electrodes [27]

EMG electrode number	Abbreviation	Name
1	PMK	Pectoralis major clavicular
2	DK	Deltoid clavicular
3	BLang	Biceps long
4	BRAD	Brachioradialis
5	DS	Deltoid scapular
6	TLang	Triceps long
7	TLat	Triceps lateral
8	TM	Triceps medial

Firstly, the subject has to place the EMG electrodes on his right arm to certain muscle groups shown in Fig. 3.13 and Table 3.6. The reason for selecting those muscle groups is that they mainly contribute to the movement of the arm. For example, the brachioradialis muscle acts to flex the forearm around the elbow joint. It can also contribute to supination and pronation of the forearm. Biceps, in addition to flexing and supinating the elbow joint it can also produce shoulder motion. In this experiment only the muscular activity of long biceps is measured. Triceps, a three-head muscle which includes long head triceps, lateral head triceps and medial head triceps is mainly responsible for extension of the elbow joint. All muscular activities on three subgroups of triceps are also recorded. At the shoulder joint the deltoid clavicular muscle and the deltoid scapular muscle are responsible for arm abduction on the frontal plane. This muscle is the antagonistic muscle of the pectoralis muscle which contributes to the adduction motion of the arm. By co-contracting all those muscles the stiffness of the arm will be increased to fulfil the task.

Perturbation

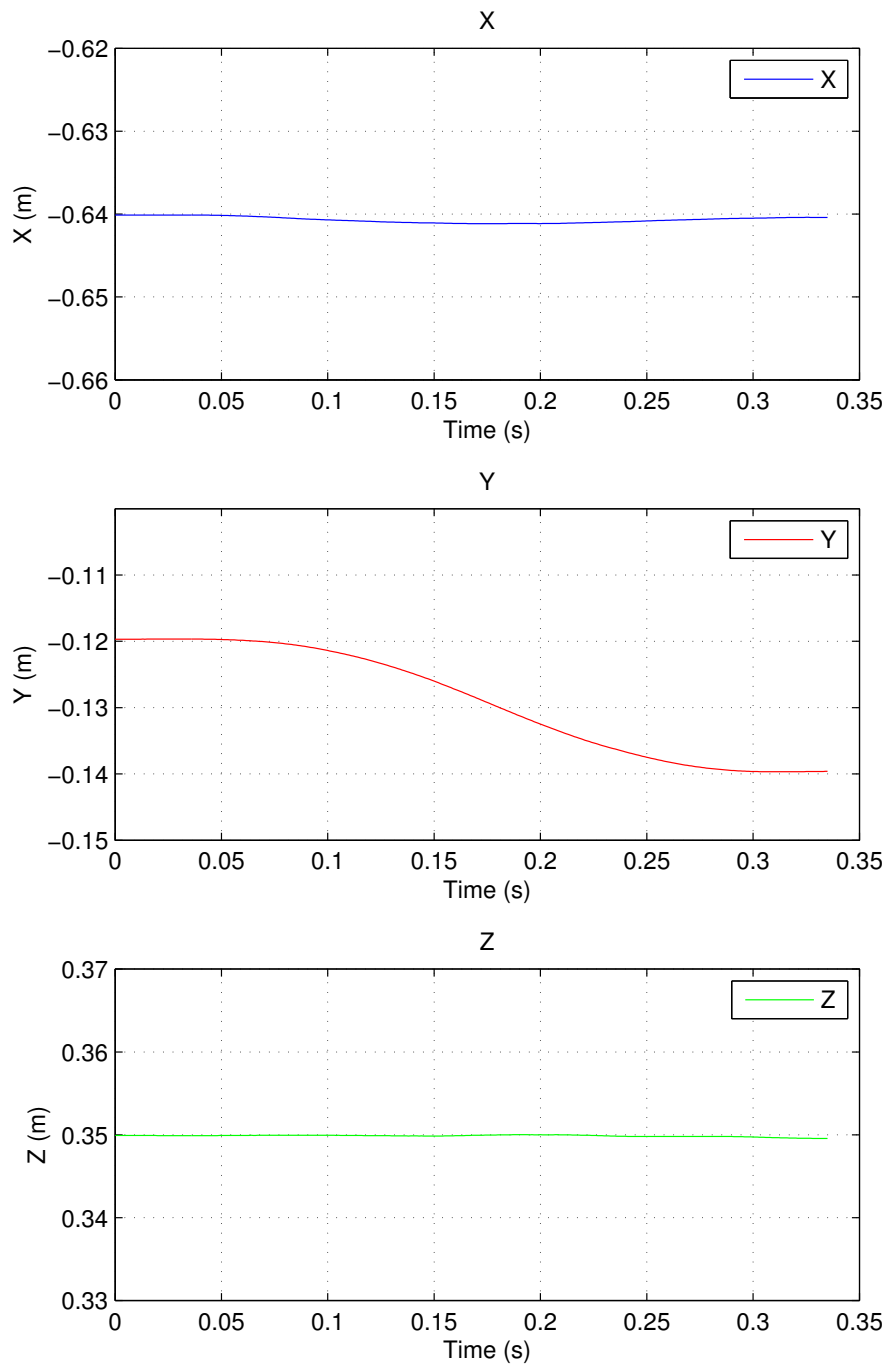


Figure 3.14.: The perturbation profile

In order to measure the human arm stiffness the perturbation of the subject's hand has to satisfy some strict requirements:

1. The perturbation must be fast and stiff enough. But with a lightweight robot the perturbation cannot be fast enough to exclude all reflexes. In this experiment the time of perturbation is about 250 ms and the joint position controller is used to control the robot.
2. The magnitude of perturbation must be small. In this experiment that value is 2 cm. The reason of this requirement is that the stiffness depends strongly on the configuration of the arm. This small displacement guarantees small changes of the arm configuration and we can assume that the stiffness is the same in the perturbation region.
3. The perturbation is done randomly in eight directions in the plane. That will avoid voluntary reaction of the subject.

To realize the perturbation, the lightweight robot uses an interpolator with minimum jerk trajectory to move the hand of the subject. To move from starting location x_s to final location x_f in time d in the plane, the minimum jerk trajectory [21] would be:

$$x(t) = x_s + (x_f - x_s) \left(10 \left(\frac{t}{d} \right)^2 - 15 \left(\frac{t}{d} \right)^4 + 6 \left(\frac{t}{d} \right)^5 \right)$$

In Fig. 3.14 it shows a typical perturbation in y direction with magnitude of 2 cm and duration of 250 ms

Force fields

The idea of using force fields is to force the subject to do different co-contraction levels that will be proportional to muscular activities of the arm. It is expected that in order to fulfil a certain task the muscular activities of the arm will be tuned according to the levels of the force fields. Two different force fields are used in the experiment, including *divergent force field* and *velocity force field*. They are similar to the force fields used in [16].

1. Divergent force field

This force field is proportional to the distance from the predefined position and the current position of the hand and has the direction from the predefined position to the current position of the hand. Mathematically, the force is computed as follows:

$$F_{divergent} = -\beta \cdot K \Delta X,$$

where β is the level of the force field and ΔX is the deviation of the end effector with respect to the predefined position. This force field acts like the spring with a negative stiffness that pushes the subject's hand away from the predefined position. Therefore, the subject must do co-contraction to counteract this force. In order to realize this force field an impedance controller with negative gains in x and y direction is exploited. However we have to cancel out the damping component in the controller. Fig. 3.15 shows forces at different locations of the end effector relative to the central predefined position.

Nevertheless, when the end effector is close to the predefined equilibrium position the force is very small that can make the subject release his muscles from co-contraction. To prevent this phenomenon a *velocity force field* will be implemented at the central area to force the subject to keep the co-contraction level.

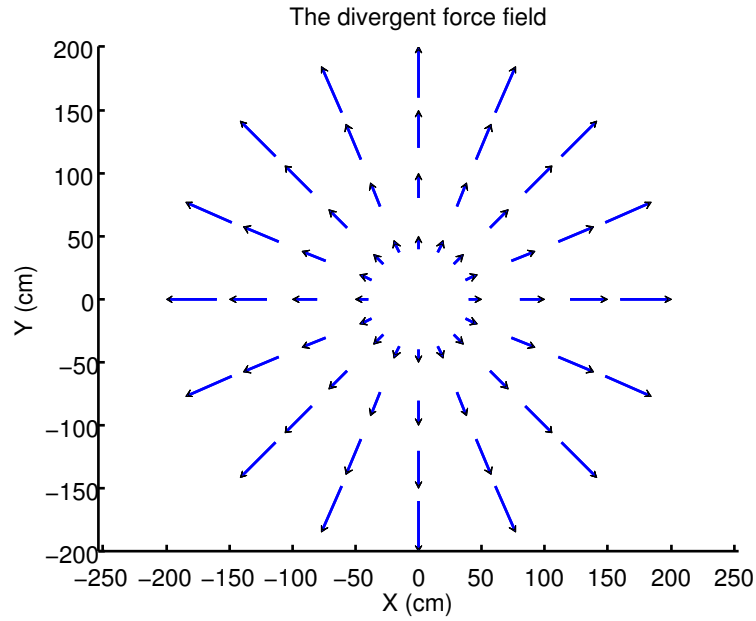


Figure 3.15.: The divergent force field

2. *Velocity force field*

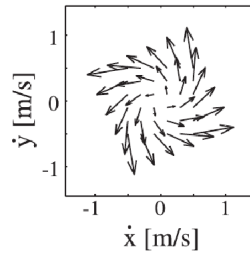


Figure 3.16.: The velocity force field [17]

During the control of the hand position the subject has to move his hand to the predefined equilibrium position. The *velocity force field* is designed in such a way that will turn away the intended velocity of the subject's movement. Mathematically, the force satisfying this purpose is as follows:

$$F_{velocity} = -\beta.KV$$

where β is the level of the force field, V is the velocity of the end effector of the lightweight robot and the gain K is chosen as:

$$K = \begin{bmatrix} 13 & -18 \\ -18 & 13 \end{bmatrix}.$$

Fig. 3.16 shows forces of this force field at different velocities of end effector.

By combining both force fields we can force the subject to keep the certain level of muscular activities by tuning the coefficient β . In this experiment four levels of the force fields are set and the end point stiffness of the arm is measured with respect to these four levels of the force field.

The task

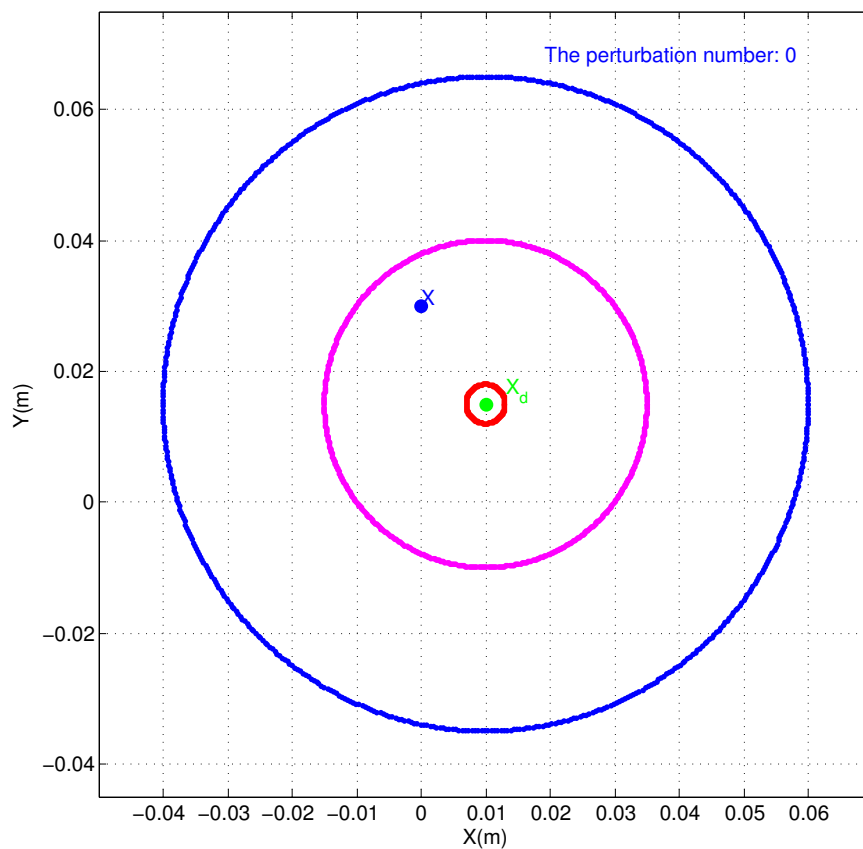


Figure 3.17.: The graphical representation to the subjects

There is one screen that displays the current position of the hand depicted as the blue point and the predefined position represented as the green point like in Fig. 3.17. The subject has to move its hand to the predefined position while both force fields are active. When the hand is in the region of 3 mm from the predefined position (the red circle) for a random time between 1 and 1.5 seconds, the lightweight robot will perturb its hand

3. *Human Arm Identification*

randomly in one of eight directions. After that it has to move out the pink circle and relax his arm muscles and repeat the task. The purpose of this is to make his muscular activity distinguishable with different levels of the two force fields.

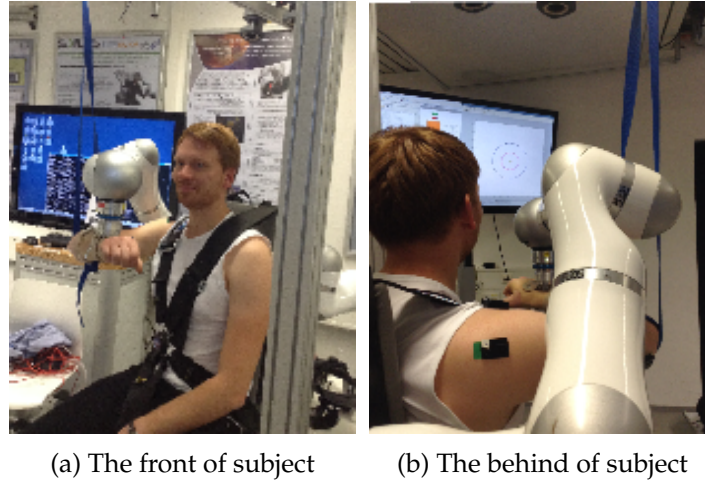


Figure 3.18.: The subject position

The whole procedure

1. *Preparation*

At the beginning, the subject's hand is mounted to the cuff as illustrated in Fig. 3.19 and the posture of the subject is shown in Fig. 3.18. Then lightweight robot is set compliantly to find out the good configuration for perturbation. The subject is instructed to do the task as described in the above section.

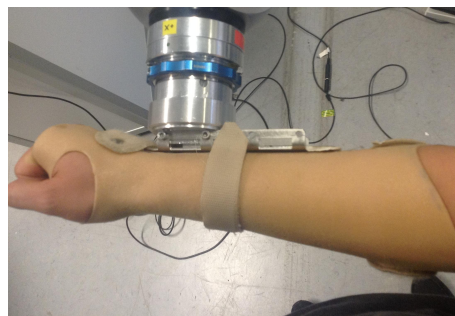


Figure 3.19.: The position of the arm in the cuff

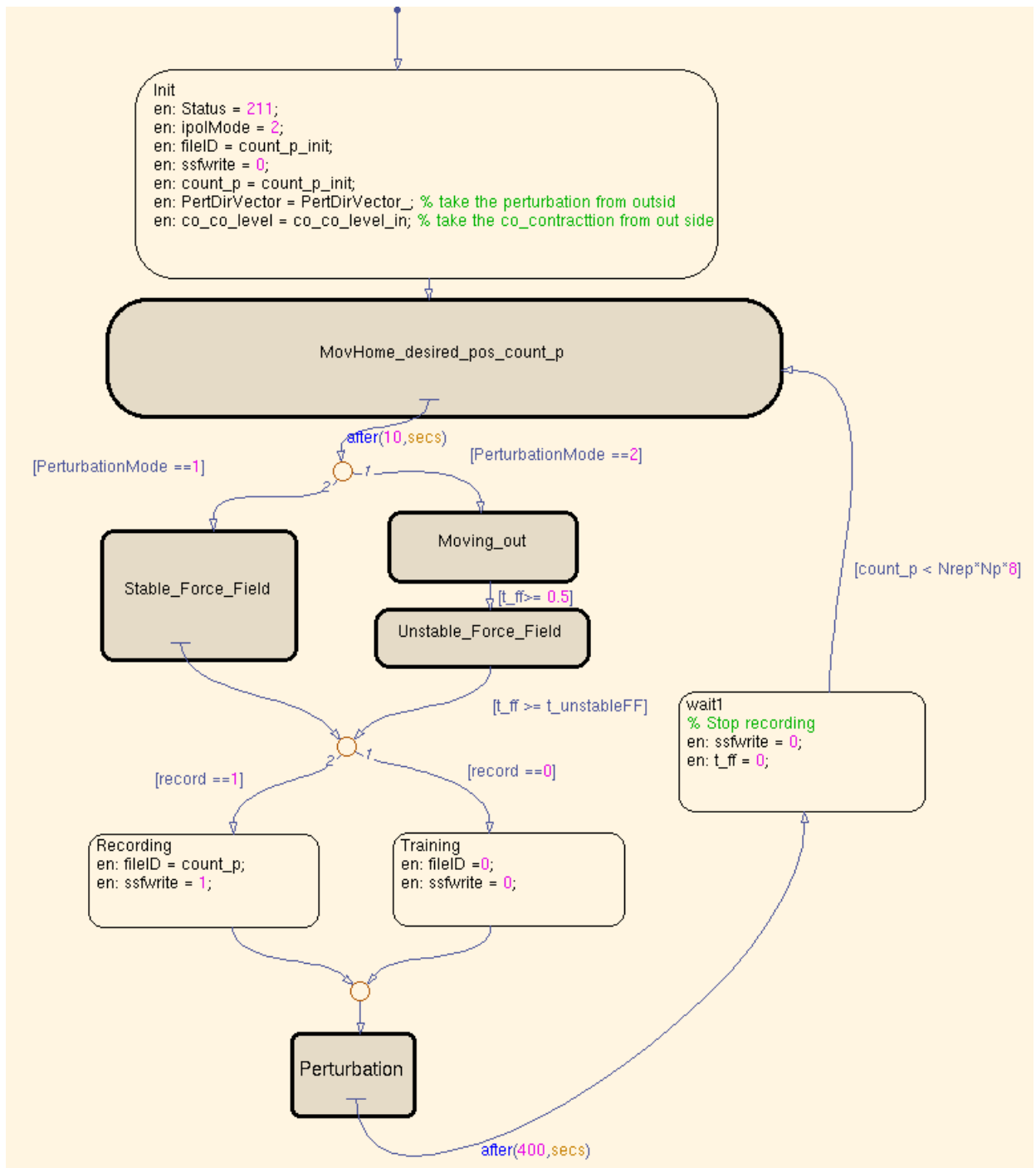


Figure 3.20.: The whole procedure of stiffness measurement

After training for a few perturbations the program will increase the level of double force fields in order to find out the maximum of the double force fields that the subject can stabilize successfully. Then the unstable force field will be designed for four different levels.

3. Human Arm Identification

Afterwards, the subject is required to be totally relaxed and the program will record the EMG data of that state for two seconds with the sampling frequency 2 KHz. This data is used for calculating EMG base noise.

2. Doing experiment

A full experiment with four levels of the force fields, eight directions of perturbations and five repetitions will be performed. The flow chart of the program is illustrated in Fig. 3.20. First, the robot moves the hand to the predefined position in the state *MovHome-desired-pos-count-p*. Then it goes to the state *Moving-out* where the subject has to move his hand out of the pink circle for 0.5 second. When he does that the state *Unstable-Force-Field* will be activated at which he has to control his arm against the force fields to reach the predefined position. Once he successes with controlling his arm staying in the red circle for a random time between 1 and 1.5 seconds the state *Recording* will be activated to start recording the EMG signals, position of the robot end effector and force torque at the end effector. Then the state *Perturbation* is active. After perturbing the arm for 400 ms the program will stop recording and go back to the state *MovHome-desired-pos-count-p*. This loop is repeated 160 times corresponding to 160 perturbations. This phase lasts about 45 minutes.

3.3.3. Data processing

Stiffness calculation

We assume that the dynamics of the hand movement follows a second order model as described in section 3.27:

$$M(t)\ddot{X}(t) + D(t)\dot{X} + K(t)(X(t) - X_0) = \Delta F(t), \quad (3.33)$$

where $X(t)$ is the hand position vector, and X_0 represents the equilibrium position. $M(t)$, $D(t)$, and $K(t)$ are hand inertia, viscosity and stiffness matrices, respectively. In order to estimate the endpoint stiffness, the arm is perturbed by a small displacement described in section 3.14. In this thesis the static stiffness is considered. We take the time windows before perturbation and after perturbation in such a way that the velocity and the acceleration of the hand are smaller than certain thresholds in order to guarantee that the inertial force and the viscous force are very negligible. Under this condition we simply have:

$$K_{static}(X(t) - X_0) = \Delta F(t) \quad (3.34)$$

By looking at each perturbation and selecting suitable time windows as shown in Fig. 3.21 the restoring force ΔF_i and the displacement ΔX_i will be extracted. The distance between two blue dash lines and between two green dash lines in Fig. 3.21 represent the selected time windows before perturbation and after perturbation. The distance between two black dash lines of the top plot in Fig. 3.21 shows the displacement of the perturbation while that of the last plot indicates the difference of the force before and after perturbation. Iterating for all perturbations a regression matrix W is formed from all displacement and the output y is formed from all restoring forces. Finally, the stiffness parameter is computed as

follows:

$$K_{static} = (W^T W)^{-1} W^T * y \quad (3.35)$$

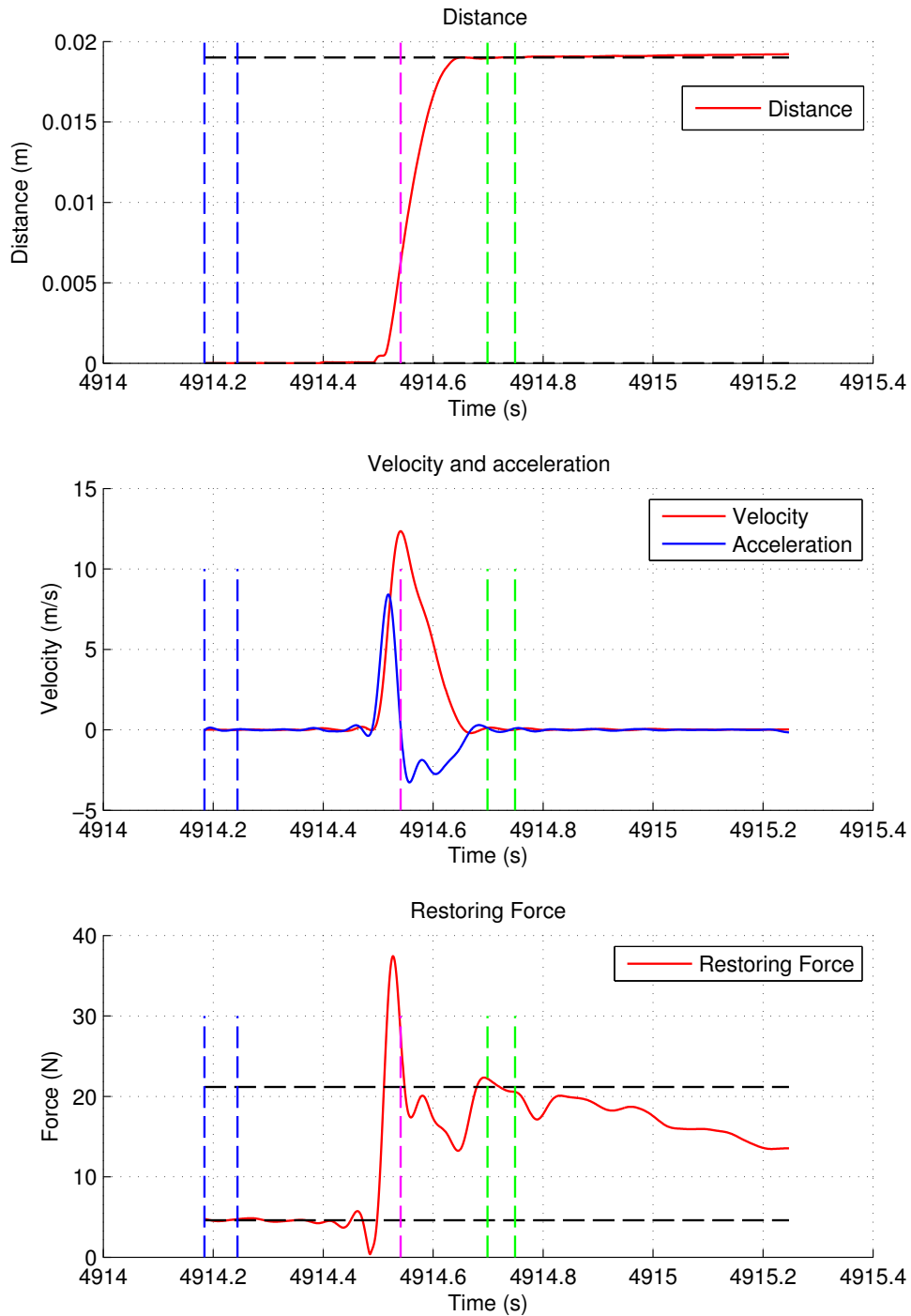


Figure 3.21.: The perturbation characteristics

3. Human Arm Identification

3.3.4. Results and discussion

Table 3.7.: The symmetric components of Cartesian stiffness matrix of subject 1

Co-contraction level	Stiffness Matrix			
	K_{11} (N/m)	K_{12} (N/m)	K_{21} (N/m)	K_{22} (N/m)
1	830	-171	-171	260
2	1041	-200	-200	281
3	1160	-183	-183	380
4	1159	-231	-231	352

Table 3.8.: The anti-symmetric components of Cartesian stiffness matrix of subject 1

Co-contraction level	anti-symmetric component			
	K_{11} (N/m)	K_{12} (N/m)	K_{21} (N/m)	K_{22} (N/m)
1	0	-54	54	0
2	0	-69	-69	0
3	0	-57	57	0
4	0	-80	80	0

Table 3.9.: The symmetric components of Cartesian stiffness matrix of subject 2

Co-contraction level	Stiffness Matrix			
	K_{11} (N/m)	K_{12} (N/m)	K_{21} (N/m)	K_{22} (N/m)
1	923	-142	-142	303
2	823	-142	-142	378
3	859	-132	-132	387
4	964	-167	-167	421

Table 3.10.: The anti-symmetric components of Cartesian stiffness matrix of subject 2

Co-contraction level	anti-symmetric component			
	K_{11} (N/m)	K_{12} (N/m)	K_{21} (N/m)	K_{22} (N/m)
1	0	-84	84	0
2	0	-83	83	0
3	0	-90	90	0
4	0	-52	52	0

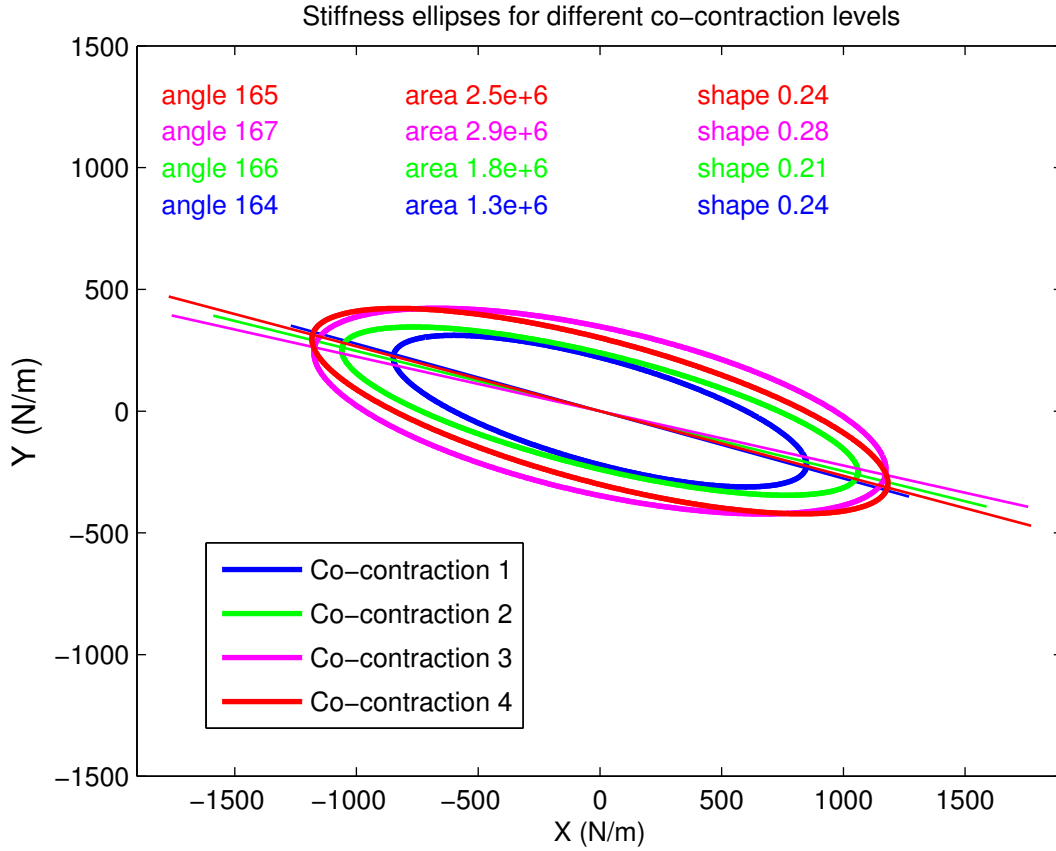


Figure 3.22.: The stiffness ellipses for different co-contraction levels of subject 1

The stiffness matrix calculated will be divided into 2 parts, including symmetric and anti-symmetric parts similar to [20].

$$K_{symmetric} = \frac{(K_{estimated} + K'_{estimated})}{2} \quad (3.36)$$

$$K_{anti-symmetric} = \frac{(K_{estimated} - K'_{estimated})}{2} \quad (3.37)$$

The symmetric matrix represents the elastic force which is related to the conservative energy which is stored in tendons or in muscles of the arm. The anti-symmetric matrix represents the non-conservative energy which is caused by the inter-muscular feedback. Fig. 3.22 and 3.23 show the stiffness estimated for different force field levels from 2 different subjects.

Each ellipse shows the restoring force with respect to the displacement of one unit. Fig. 3.22, 3.23 and 3.24 and Tables 3.7, 3.8, 3.9 and 3.10 indicate the following characteristics of the arm stiffness:

- The conservative component of the stiffness matrix is much bigger than the non-conservative one both in size (approximately 10 times). This indicates that the arm

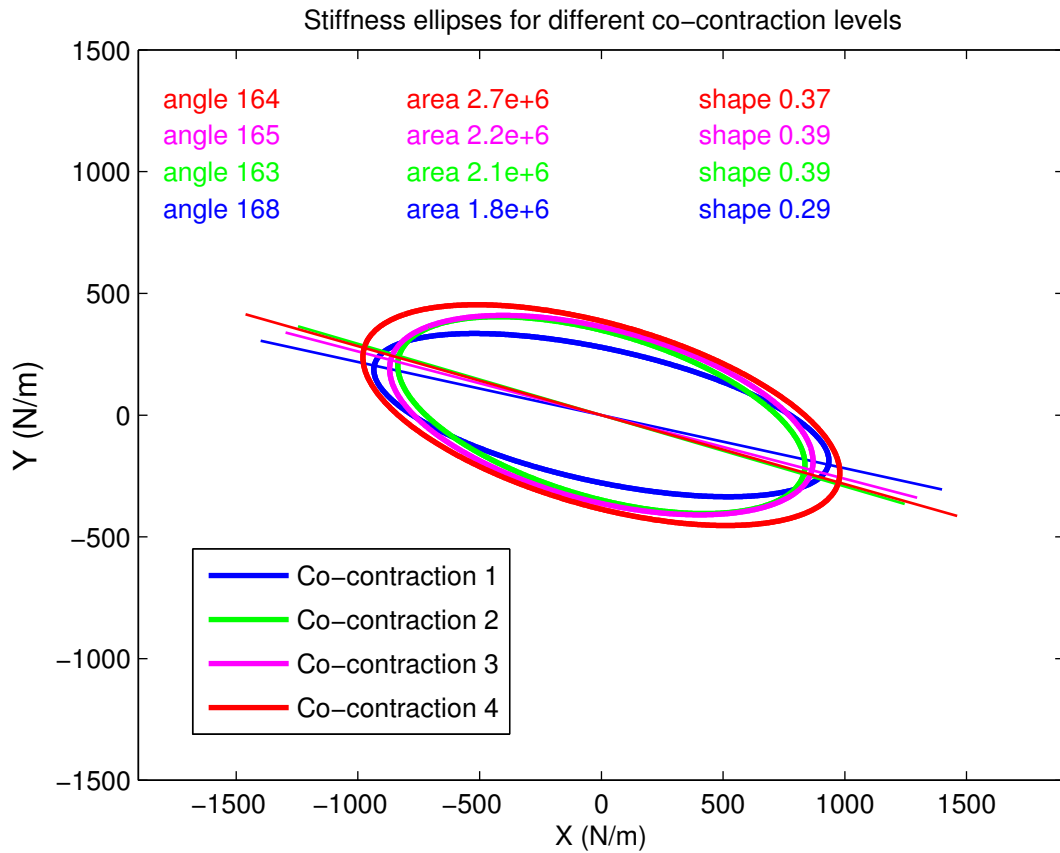


Figure 3.23.: The stiffness for different co-contraction levels of subject 2

is predominantly *spring-like*. It is consistent with the result found by Mussa Ivaldi in [20]. This property can be explained by the elastic property of the tendons and muscles of the arm. In terms of energy consumption, this property allows saving energy and releasing it during movement [11]

- The stiffness ellipse increases in size according to the force field level and keeps almost the same orientation (Fig. 3.22, Fig. 3.23). It seems that the central nervous system modulates the stiffness by increasing overall stiffness using co-contraction of all muscles rather than selecting some of them to counteract the force field. This strategy is reasonable because the force field is divergent in all directions in the plane for the first measurement.
- The learning is quite clear in the second measurement in Fig. 3.24 . With the same setup for the force field levels and the same location of the hand, the later stiffness is significantly smaller in major direction. This shows that the subject keep the same level of stiffness in minor direction and reduce the stiffness in major direction to minimize the metabolic cost. The further investigation of learning process with the force field is not the scope of this thesis.

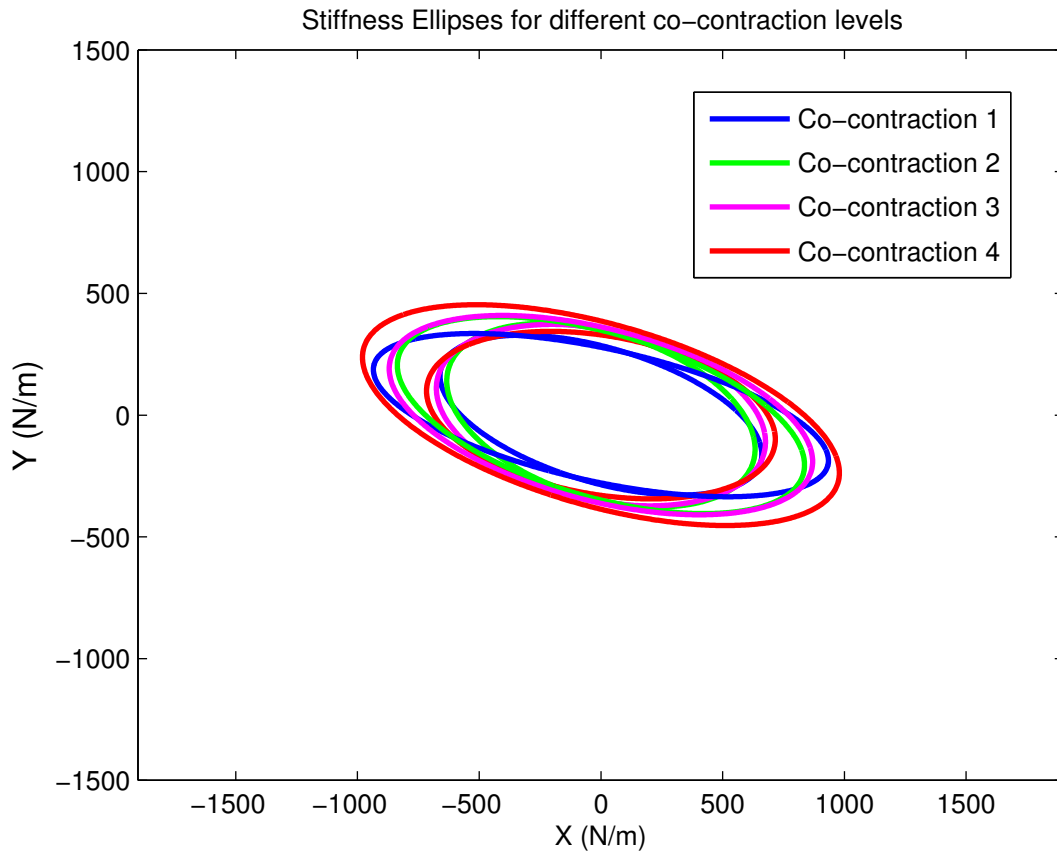


Figure 3.24.: The indication of learning in control stiffness. Four outside ellipses are earlier stiffness while four inside ellipses are the later stiffness

However we can see that the stiffness of subject 2 at four different levels of force field is not so differentiable. It can be explained that the subject might apply the quite similar strategy for different levels of force fields. This is possible because the direction and the levels of force fields are randomly chosen. For example, it can apply the quite high co-contraction levels of muscle even if the force field level is small. This can be reduced to a certain extent by forcing the subject to relax before trying a new task.

4. Calibration of human arm stiffness and surface EMG signals

In this chapter processing of EMG signals will be presented. Then the discussion of correlation between EMG data and endpoint stiffness is given. Consequently, two methods of *Least Squares Regression* and *Regularized Least Squares* to estimate the endpoint stiffness on-line from EMG signals will be described. Finally, a simple practical method of linearisation of the endpoint stiffness according to the sum of all EMG signals is also mentioned.

4.1. EMG processing

Surface EMG signal is measured by EMG electrode placed on the skin. This signal is superposition of motor unit action potentials. It is noted that this signal is well correlated with the force the muscle is exerting.

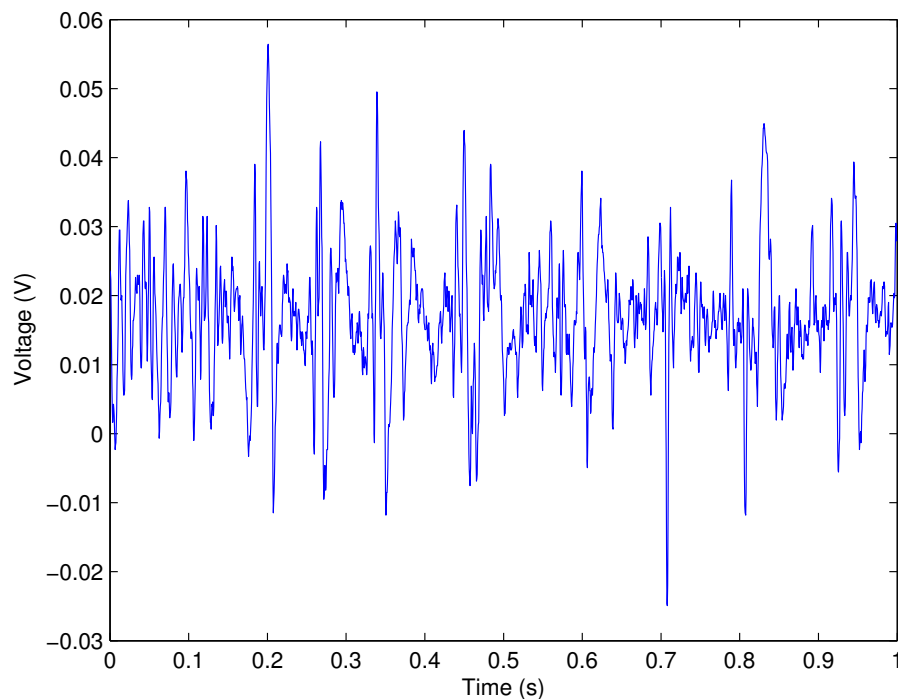


Figure 4.1.: The raw EMG signal of one channel

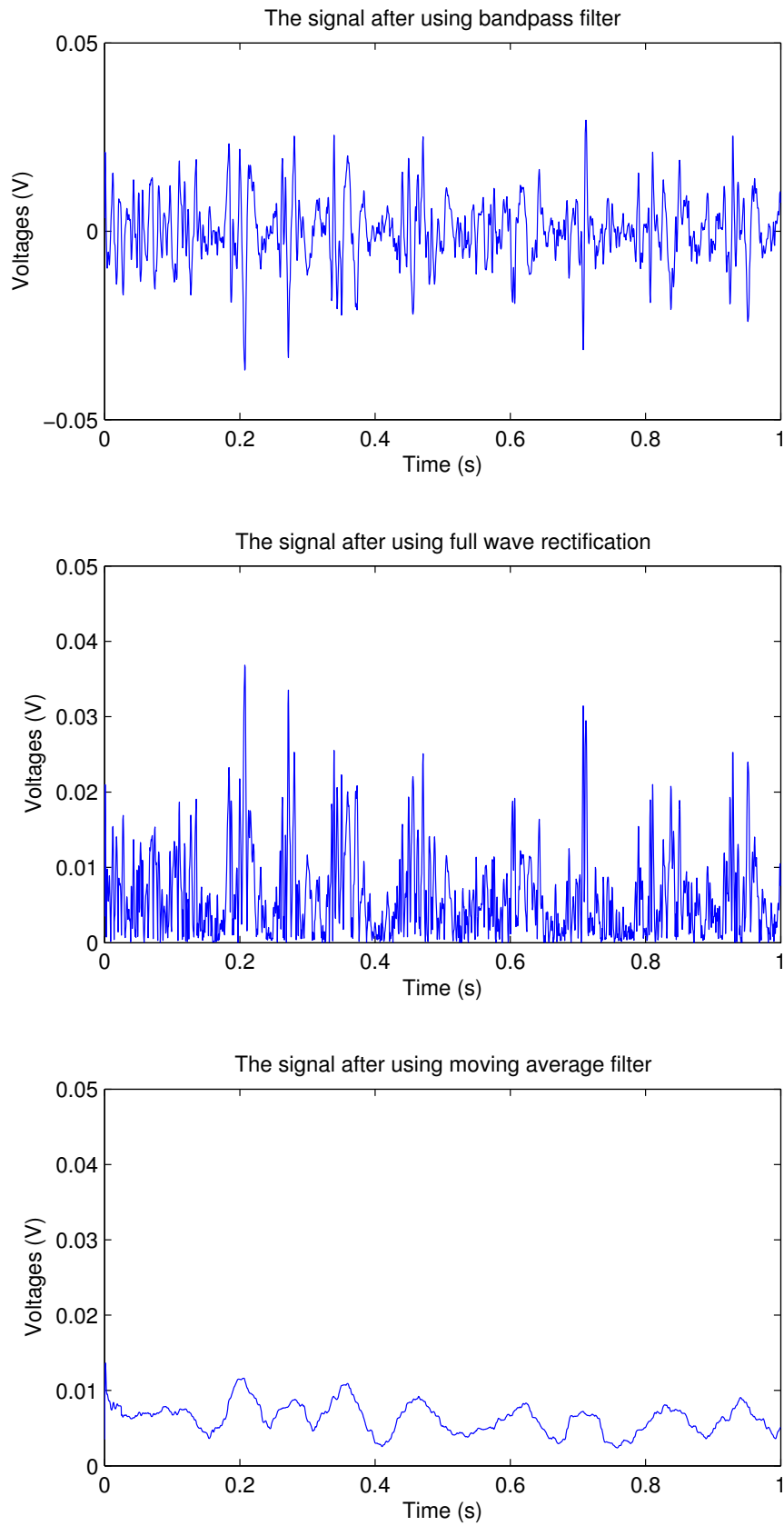


Figure 4.2.: The processed EMG

4. Calibration of human arm stiffness and surface EMG signals

The raw EMG signals of eight electrodes are recorded before each perturbation. Fig. 4.1 illustrates one example of those signals. It can be seen that the signal has an offset value which should be subtracted. The following processing steps are applied to raw data:

1. *Bandpass filter*: Filter the data with *bandpass* filter with frequency range of [25-500]Hz. A Butterworth 3rd order filter in Matlab is used to realize this filter. After this step the offset of the signal is removed as shown in Fig. 4.2 .
2. *Averaged rectified value*: The signal from the first step is further processed using *full wave rectification*. Then *Moving average filter* is employed. The result is presented in Fig. 4.2.
3. *Mean calculation*: Calculate the mean value of the time window 50 ms before perturbation and subtract the base noise.

The EMG data when the subject is totally resting is used to calculate the base noise. This value is then subtracted for each perturbation.

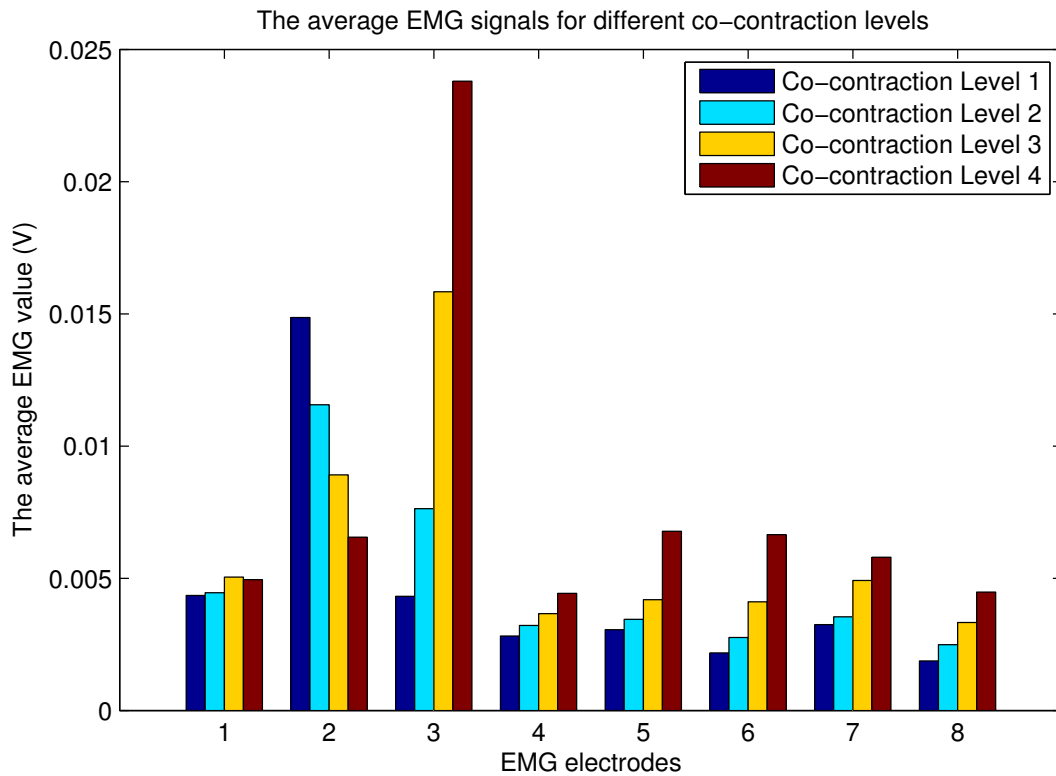


Figure 4.3.: The EMG signals (number according to the Table 3.6 at page 28)

After processing the EMG data for each level of the force fields, the result is represented in Fig. 4.3. The horizontal axis represents electrodes number according to the definition in Table 3.6 and the columns for each number represent the average EMG signals corresponding four different force field levels. It is shown that the subject used *biceps long head*,

triceps long head and *triceps medial* more than other muscle groups in order to stabilize his hand in the plane. In each muscle group it is quite clear that the muscular activity increases monotonically to the force field level, except EMG_2 . Table 4.1 shows the correlation values between the stiffness elements and EMG signals. We can see that K_{11} and K_{22} have good correlation with EMG signals as indicated by symbol "*" in the table. For not asterisk cell's H_0 can be rejected, that the correlation is not significant. Therefore we assume a linear model between stiffness elements K_{11} and K_{22} and EMG signals (8×1).

Table 4.1.: The correlation value between stiffness elements and EMG signals

Correlation	EMG_1	EMG_2	EMG_3	EMG_4	EMG_5	EMG_6	EMG_7	EMG_8
K_{11}	0.92	-0.98*	0.99*	0.98*	0.92	0.97*	0.99*	0.99*
K_{12}	0.14	0.24	-0.07	-0.18	-0.13	-0.10	0.01	-0.16
K_{21}	-0.51	0.85	-0.79	-0.86	-0.83	-0.82	-0.73	-0.84
K_{22}	0.88	-0.99*	0.99*	0.99*	0.94	0.98*	0.99*	0.99*

4.2. Least Squares Regression

4.2.1. Concept

We observe a system which generates scalar output $y \in \mathbb{R}$ from input vector $x \in \mathbb{R}^d$. By collecting data in the working range of the system, we obtain a set of data $S = \{(x_1, y_1), \dots, (x_N, y_N)\}$. From this data set we have to find a function $f: \mathbb{R}^d \mapsto \mathbb{R}$ that can predict the output of the system for any arbitrary input vector x . In the case of linear relation, we have prediction as follows:

$$\hat{y} = w^T x, \quad (4.1)$$

where w is a weight vector in \mathbb{R}^d . The mean squared error between prediction output and actual output is as follows:

$$MSE = \frac{1}{N} \sum_1^N (y_i - \hat{y}_i)^2 = \frac{1}{N} \sum_1^N (y_i - w^T x_i)^2. \quad (4.2)$$

We have to find the w value such that the objective function as mean squared error is minimized. This leads to a convex optimization problem of w as:

$$\arg \min_w MSE(w) = \frac{1}{N} \sum_1^N (y_i - w^T x_i)^2. \quad (4.3)$$

By setting the partial derivative of $MSE(w)$ with respect to w equal to zero:

$$\frac{\partial MSE(w)}{\partial w} = 0, \quad (4.4)$$

we achieve the solution of Eq. (4.3) as follows:

$$w = (X^T X)^{-1} X^T Y, \quad (4.5)$$

where

$$X = \begin{pmatrix} x_1^T \\ x_2^T \\ \dots \\ x_N^T \end{pmatrix}, Y = \begin{pmatrix} y_1 \\ y_2 \\ \dots \\ y_N \end{pmatrix}.$$

4.2.2. Application of Least Squares Regression

In this particular problem, mapping EMG signals to the human arm endpoint stiffness, we have a process with input consisting of 8 EMG signals and output is one of four elements of the stiffness matrix. With four co-contraction levels we arrange data as follows:

$$K_{11} = \begin{pmatrix} K_{11/coco1} \\ K_{11/coco2} \\ K_{11/coco3} \\ K_{11/coco4} \end{pmatrix}, K_{12} = \begin{pmatrix} K_{12/coco1} \\ K_{12/coco2} \\ K_{12/coco3} \\ K_{12/coco4} \end{pmatrix}, K_{21} = \begin{pmatrix} K_{21/coco1} \\ K_{21/coco2} \\ K_{21/coco3} \\ K_{21/coco4} \end{pmatrix}, K_{22} = \begin{pmatrix} K_{22/coco1} \\ K_{22/coco2} \\ K_{22/coco3} \\ K_{22/coco4} \end{pmatrix},$$

$$X = \begin{pmatrix} EMG_{1/coco1} & EMG_{2/coco1} & \dots & EMG_{8/coco1} & 1 \\ EMG_{1/coco2} & EMG_{2/coco2} & \dots & EMG_{8/coco2} & 1 \\ EMG_{1/coco3} & EMG_{2/coco3} & \dots & EMG_{8/coco3} & 1 \\ EMG_{1/coco4} & EMG_{2/coco4} & \dots & EMG_{8/coco4} & 1 \end{pmatrix}$$

$$w_{11} = \begin{pmatrix} w_{1/11} \\ w_{2/11} \\ \dots \\ w_{9/11} \end{pmatrix}, w_{12} = \begin{pmatrix} w_{1/12} \\ w_{2/12} \\ \dots \\ w_{9/12} \end{pmatrix}, w_{21} = \begin{pmatrix} w_{1/21} \\ w_{2/21} \\ \dots \\ w_{9/21} \end{pmatrix}, w_{22} = \begin{pmatrix} w_{1/22} \\ w_{2/22} \\ \dots \\ w_{9/22} \end{pmatrix},$$

Where $K_{ij/cocok}$ is the element (i, j) of the stiffness matrix with respect to the co-contraction level k , $w_{k/ij}$ is the k -th linear coefficient corresponding to the stiffness element $K(i, j)$, and $EMG_{k,cocoi}$ is the k -th EMG element corresponding to co-contraction level i .

Applying *Least squares Regression* we have:

$$w_{11} = (X^T X)^{-1} X^T K_{11} \quad (4.6)$$

$$w_{12} = (X^T X)^{-1} X^T K_{12} \quad (4.7)$$

$$w_{21} = (X^T X)^{-1} X^T K_{21} \quad (4.8)$$

$$w_{22} = (X^T X)^{-1} X^T K_{22} \quad (4.9)$$

Here is one of example of w after calibrating for one subject:

$$w = \begin{pmatrix} 4.2e3 & -4.2e3 & 11e3 & -1.1e3 & -8.4e3 & -4.4e3 & 4.1e3 & -6.8e2 & 3.1e2 \\ 4.4e3 & 11.2e3 & 6.7e3 & -2.5e3 & -8.4e3 & -4.7e3 & 4.8e3 & -2.7e3 & -2.7e2 \\ 5.4e3 & 11.3e3 & 6.2e3 & -3.1e3 & -11.3e3 & -6.7e3 & 5.5e3 & -3.3e3 & -2.8e2 \\ -3.3e2 & -4.3e3 & 2.0e3 & 5.9e2 & 1.0e3 & 8.4e2 & -2.6e2 & 7.9e2 & 1.9e2 \end{pmatrix}$$

4.2.3. Online estimation of arm stiffness

After calculating w for all elements of the stiffness matrix, the human arm stiffness can be computed as:

$$\begin{pmatrix} K_{11} \\ K_{12} \\ K_{21} \\ K_{22} \end{pmatrix} = \begin{pmatrix} w_{11}^T \\ w_{12}^T \\ w_{21}^T \\ w_{22}^T \end{pmatrix} \begin{pmatrix} EMG_1 \\ EMG_2 \\ \dots \\ EMG_8 \\ 1 \end{pmatrix} \quad (4.10)$$

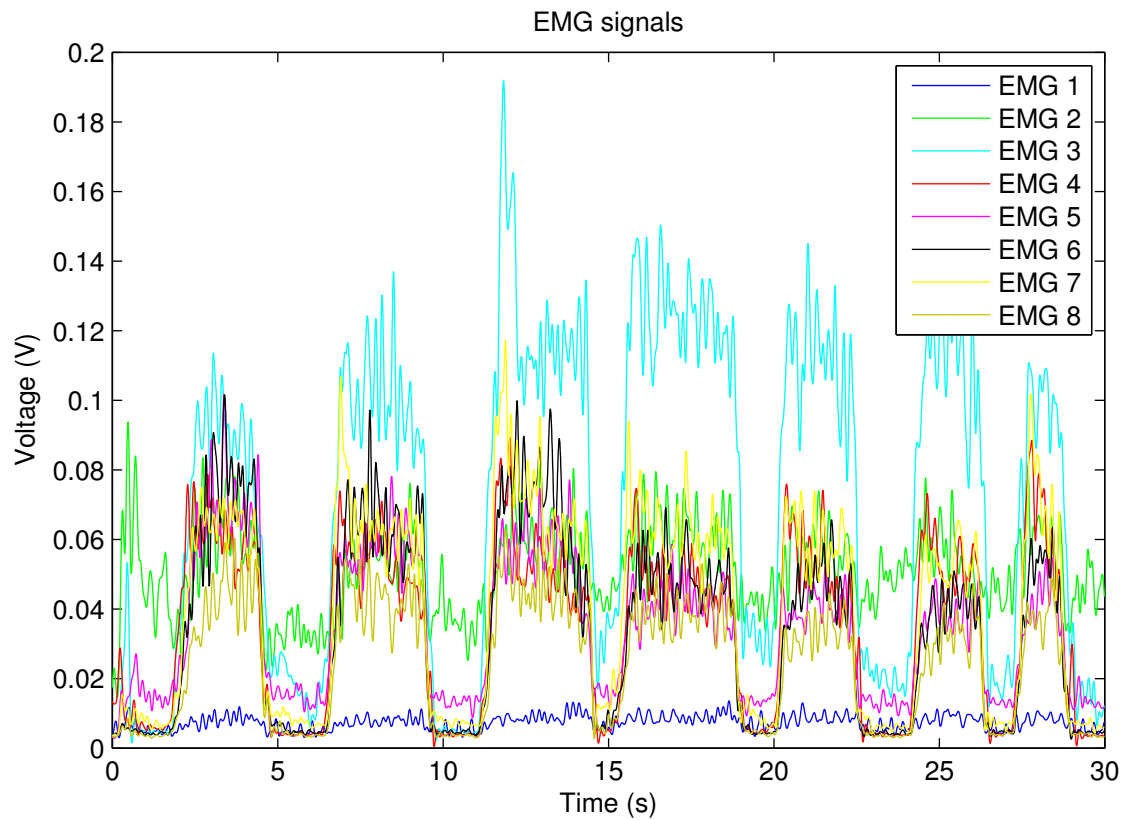


Figure 4.4.: The processed EMG signals

The subject holds his arm at the calibrated configuration and does cocontraction for several seconds and then releases for several seconds. The EMG signals are processed online according to the following steps:

1. Bandpass filter with frequency range [25-500] Hz
2. Full wave rectifier

3. Moving average filter
4. Lowpass filter with cutoff frequency 1.5 Hz

Fig. 4.4 illustrates the output EMG signals. It can be seen that when the subject does cocontraction the EMG signals of all muscle increase. And when he releases those signals decrease respectively.

The corresponding estimated stiffness according to Eq. (4.10) is shown in Fig. 4.5. All the stiffness elements change according to EMG signals and their variances are relatively high. Especially, it is quite clear that K_{11} and K_{22} increase when EMG signals increase. K_{21} and K_{12} have no correlation with EMG signals as indicated in Table 4.1. Therefore, we cannot give any conclusion about these elements of the stiffness matrix.

The large variance can be explained by the reason that the w value is significantly large. When it is multiplied with much varying EMG signals, the resulting stiffness is varying quite a lot.

4.3. Regularized Least Squares

4.3.1. Concept

Similar to the Least Squares Regression method, the Regularized Least Squares method adds an regularization term which is proportional to the square of w to the mean squared error function. That leads to an objective function [18] as follows:

$$F(w) = \frac{1}{2N} \sum_1^N (y_i - \hat{y}_i)^2 + \frac{1}{2} \lambda \|w\|^2. \quad (4.11)$$

Using the same method as mentioned in section 4.2, setting the partial derivative of $F(w)$ with respect to w equal to zero:

$$\frac{\partial F(w)}{\partial w} = 0, \quad (4.12)$$

we obtain the solution of Eq. (4.11) as follows:

$$w = (X^T X + \lambda I_d)^{-1} X^T Y, \quad (4.13)$$

where I_d is a d dimension identity matrix and X and Y are defined as in section 4.2. In comparison to the Least Squares Regression this method introduces the term λI_d in the solution that regulates the magnitude of w . When the λ value is large w will be small and vice versa. By tuning λ we can achieve different w .

4.3.2. Application of Regularized Least Squares

Using the same notation as in section 4.2, the w values for all elements of stiffness matrix can be computed as follows:

$$w_{11} = (X^T X + \lambda_{11} I_d)^{-1} X^T K_{11} \quad (4.14)$$

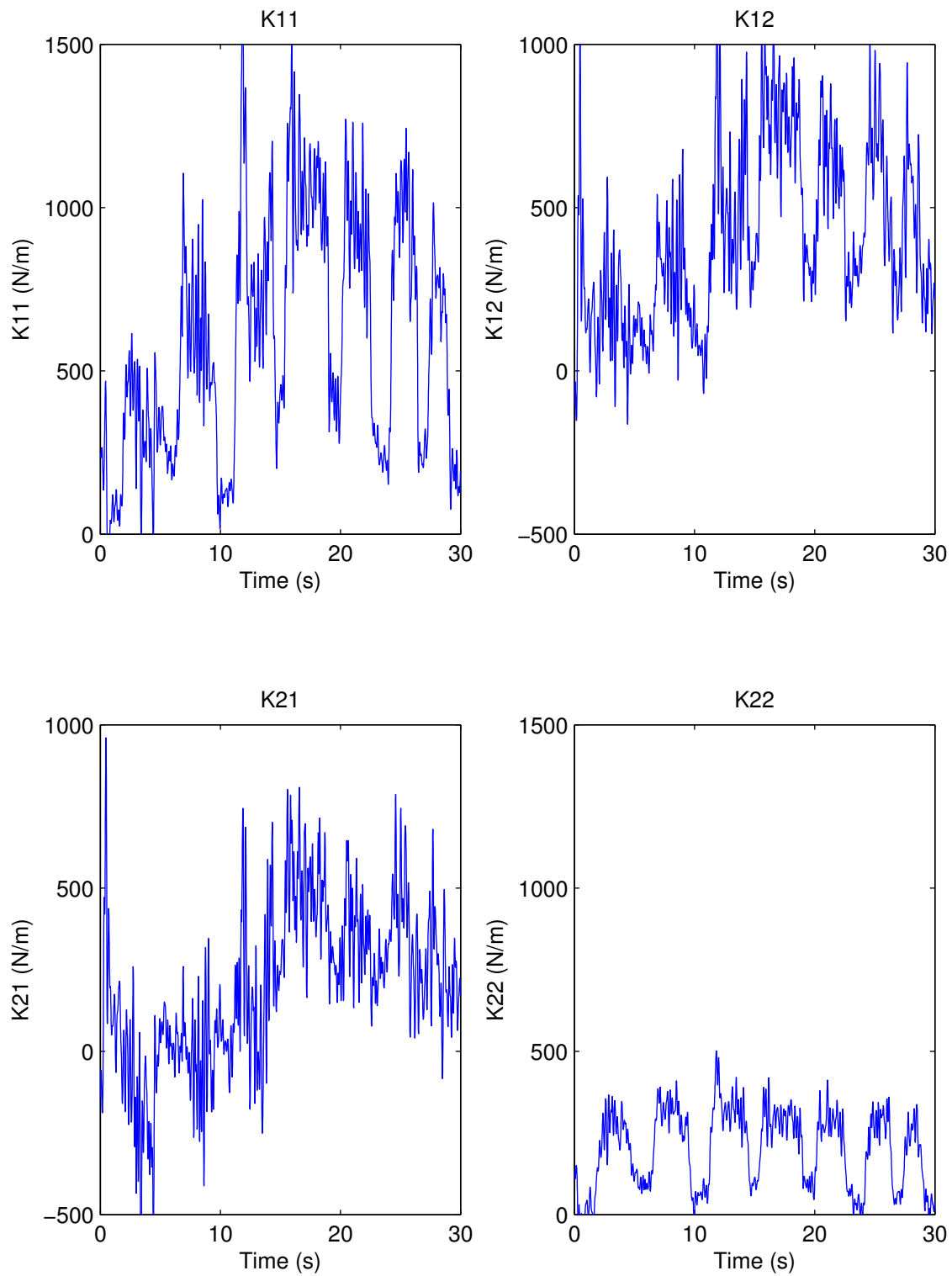


Figure 4.5.: The estimated stiffness from EMG signals using Least Squares Regression

$$w_{12} = (X^T X + \lambda_{12} I_d)^{-1} X^T K_{12} \quad (4.15)$$

$$w_{21} = (X^T X + \lambda_{21} I_d)^{-1} X^T K_{21} \quad (4.16)$$

$$w_{22} = (X^T X + \lambda_{22} I_d)^{-1} X^T K_{22} \quad (4.17)$$

4.3.3. Online estimation of the arm stiffness

After calculating w value for all elements of the stiffness matrix, the human arm stiffness can be computed as:

$$\begin{pmatrix} K_{11} \\ K_{12} \\ K_{21} \\ K_{22} \end{pmatrix} = \begin{pmatrix} w_{11}^T \\ w_{12}^T \\ w_{21}^T \\ w_{11}^T \end{pmatrix} \begin{pmatrix} EMG_1 \\ EMG_2 \\ \dots \\ EMG_8 \\ 1 \end{pmatrix} \quad (4.18)$$

The same EMG signals shown in Fig. 4.4 are used to estimate stiffness

Case 1

$$\lambda_{11} = 0.001, \lambda_{12} = 0.001, \lambda_{21} = 0.001, \lambda_{22} = 0.001$$

The calculated w :

$$\begin{pmatrix} 72 & -757 & 1.9e3 & 148 & 333 & 415 & 259 & 242 & 365 \\ 1 & 22 & -13 & -4 & -6 & -5 & 1 & -5 & -101 \\ -7 & 122 & -275 & -25 & -57 & -66 & -34 & -39 & -128 \\ 29 & -299 & 740 & 59 & 134 & 165 & 101 & 96 & 169 \end{pmatrix}$$

Case 2

$$\lambda_{11} = 0.0005, \lambda_{12} = 0.0005, \lambda_{21} = 0.0005, \lambda_{22} = 0.0005$$

The calculated w :

$$\begin{pmatrix} 117 & -1.2e3 & 3.1e3 & 239 & 537 & 672 & 422 & 393 & 351 \\ 3 & 42 & -18 & -6 & -10 & -8 & 3 & -8 & -101 \\ -10 & 204 & -444 & -40 & -95 & -109 & -54 & -64 & -126 \\ 43 & -491 & 1.2e3 & 96 & 218 & 268 & 163 & 156 & 164 \end{pmatrix}$$

In comparison to the w value in the method Least Squares Regression, the values obtained by Regularized Least Squares in both cases are much smaller. The estimated stiffness elements are shown in Fig. 4.6 and Fig. 4.7.

We can see that the stiffness elements are not much varying in comparison to those of Least Squares Regression method. K_{21} and K_{12} is almost not changed when the subject does co-contraction since w_{12} and w_{21} are quite small. K_{11} and K_{22} change according to the EMG signals and always positive. Therefore, those stiffness values can be applied to the controller of the slave robot.

When λ converges to zero, w value becomes larger and the estimated stiffness varies a lot. From above analysis the method Regularized Least Squares is chosen to estimate stiffness with $\lambda_{11} = 0.001, \lambda_{12} = 0.001, \lambda_{21} = 0.001, \lambda_{22} = 0.001$.

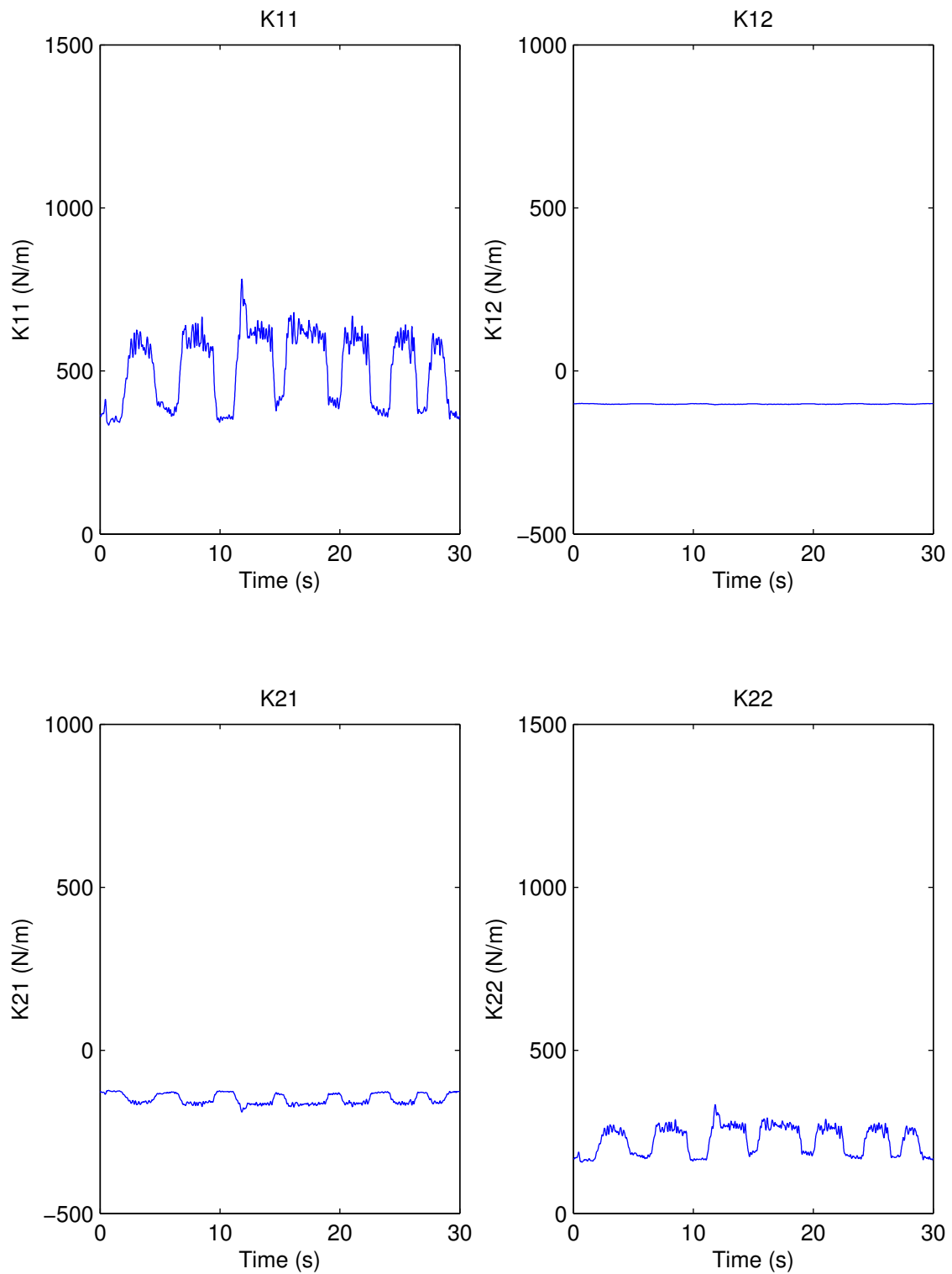


Figure 4.6.: The estimated stiffness from EMG signals using Regularized Least Squares
 $\lambda_{11} = 0.001, \lambda_{12} = 0.001, \lambda_{21} = 0.001, \lambda_{22} = 0.001$

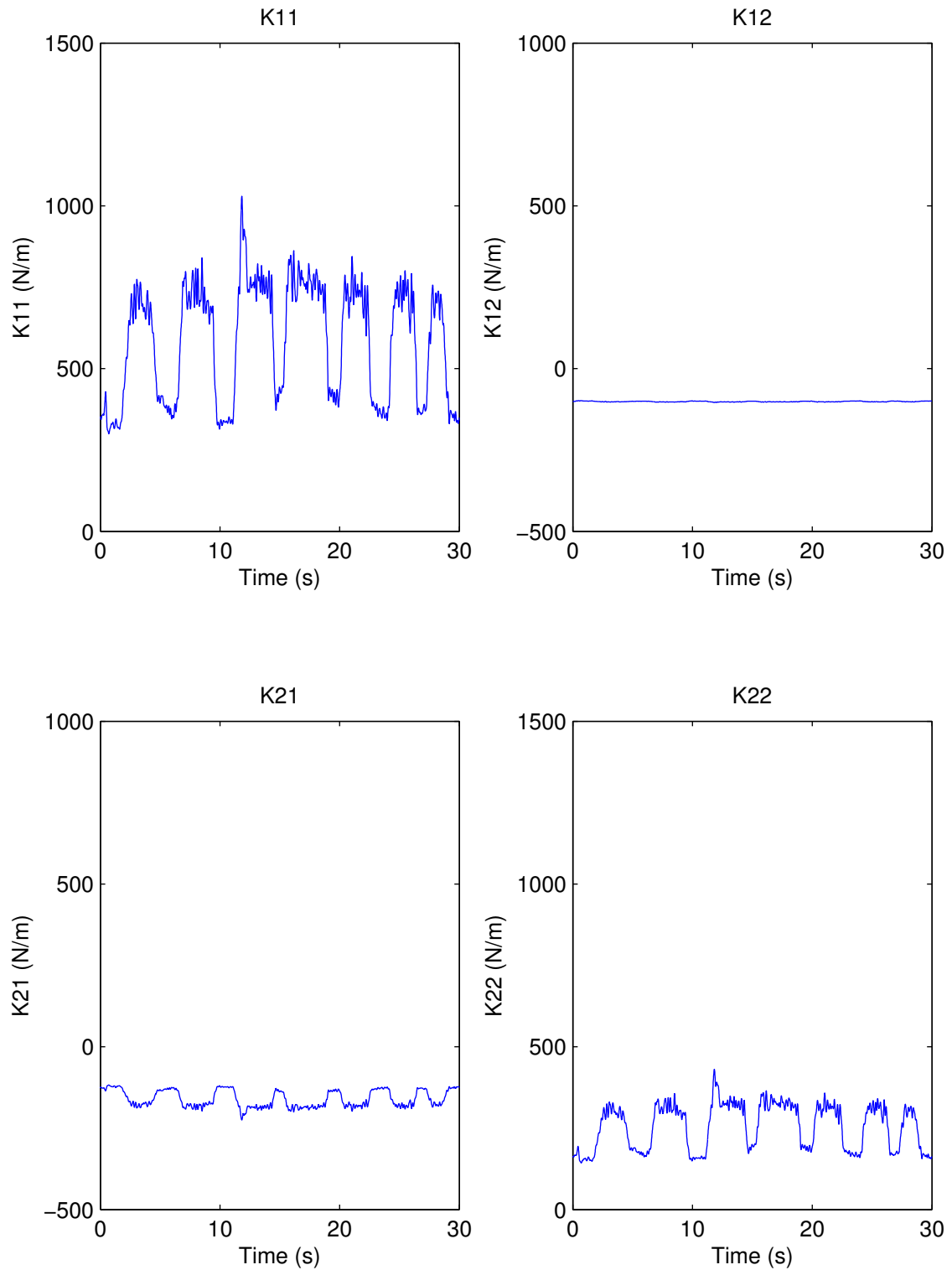


Figure 4.7.: The estimated stiffness from EMG signals using Regularized Least Squares
 $\lambda_{11} = 0.0005, \lambda_{12} = 0.0005, \lambda_{21} = 0.0005, \lambda_{22} = 0.0005$

4.4. Linearisation the stiffness matrix according to the sum of EMG signals

For simplicity, the processed EMG signals is summed up to a single number α which corresponds to the co-contraction level that the arm does. The diagonal stiffness matrix in 3D can be scaled linearly according to this value as follows.

$$Kx = Kx_{min} + \frac{\alpha - \alpha_{min}}{\alpha_{max} - \alpha_{min}}(Kx_{max} - Kx_{min}) \quad (4.19)$$

$$Ky = Ky_{min} + \frac{\alpha - \alpha_{min}}{\alpha_{max} - \alpha_{min}}(Ky_{max} - Ky_{min}) \quad (4.20)$$

$$Kz = Kz_{min} + \frac{\alpha - \alpha_{min}}{\alpha_{max} - \alpha_{min}}(Kz_{max} - Kz_{min}) \quad (4.21)$$

where α_{min} is the sum of EMG signals when the subject's arm is totally relaxed and α_{max} is the sum of EMG signals when the subject does highest cocontraction as possible. Kx_{min} , Ky_{min} , Kz_{min} , Kx_{max} , Ky_{max} , Kz_{max} can be selected as $Kx_{min} = Ky_{min} = Kz_{min} = 200$ (N/m) and $Kx_{max} = Ky_{max} = Kz_{max} = 2000$ (N/m). They are assumed to be the minimal and maximal stiffness of the subject's arm in x, y, and z directions. Other off-diagonal elements in the stiffness matrix are set to zero. The above values can be applied directly to the controller of the slave robot. This is a very simple method to scale the stiffness of the slave robot with the EMG signals from human operator. The advantage of this simple method is that we do not need to measure human stiffness but scale stiffness directly from EMG signals. In this way, the human operator can vary the endpoint stiffness of the slave robot by co-contracting the muscle on his arm.

5. Teleoperation

In this chapter, the model of teleoperation system is given. The main focus is the practical implementation of EMG based bilateral controller.

5.1. The model of the teleoperation system

The teleoperator consists of a *master* and a *slave* robotic system at which the *slave* robot tries to imitate the behaviour of the *master* robot. The human operator controls the slave robot through master robot in order to fulfil different type of tasks. Basically, in bilateral teleoperation the *master* robot sends its position and/or velocity to the *slave* robot and in return, the slave robot will send the force feedback to the master robot. In this way, the human operator can feel the interacting force and torque at the slave side. The teleoperation system with 2 lightweight robots can be modelled as the following equations [23]:

$$\begin{cases} \Lambda_m(q_m)\ddot{x}_m + \mu_m(q_m, \dot{q}_m)\dot{x}_m + J(q_m)^{-T}g(q_m) = J(q_m)^{-T}\tau_m + F_h \\ \Lambda_s(q_s)\ddot{x}_s + \mu_s(q_s, \dot{q}_s)\dot{x}_s + J(q_s)^{-T}g(q_s) = J(q_s)^{-T}\tau_s - F_e \end{cases} \quad (5.1)$$

where F_h and F_e are the forces and torques caused by human operator and the environment respectively. Other notations have the same meanings as Eq. (2.26) but they apply for master robot and slave robot.

With the EMG based bilateral controller, the behaviour of the slave robot can also be modulated in a way that the stiffness of the arm of the human operator estimated from EMG signals will be applied to the controller of the slave robot. This allows the slave robot to mimic the stiffness of the human arm. Therefore, the human operator can flexibly change the stiffness of the slave robot to interact effectively with unknown and unstructured environments.

5.2. Implementation

The EMG based bilateral scheme with force feedback is illustrated in Fig. 5.1 with two lightweight robots. On the master side, the master robot LBR3 is driven by the force F_h introduced by the human operator and the force produced by its controller which comprises the gravity force and feedback force from the slave robot. On the slave side, the slave controller takes position error between the position from the master robot as the desired position x_m and its current position x_s to produce the force F_s . This force, along with the environmental force F_e drive the slave robot LBR4. The slave controller is Cartesian impedance controller which takes the stiffness from the EMG-based stiffness estimator. According to this scheme, the human operator can feel the interactive force between the environment and the slave robot and transfer his reaction to the controller of the slave robot in terms of human stiffness and desired position.

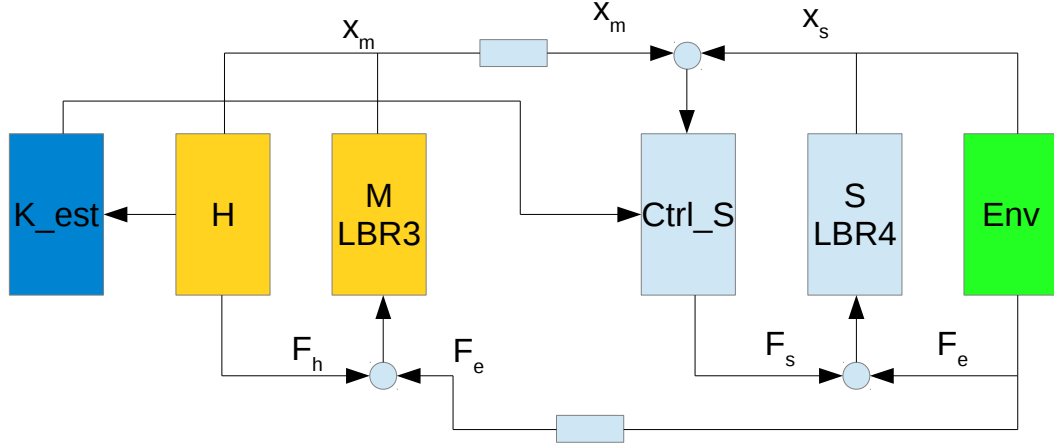


Figure 5.1.: EMG based bilateral controller [24]

5.2.1. Coordinate Transformation in teleoperation

In teleoperation the movement of the slave robot should be made the same as that of the master robot. In order to realize the teleoperation scheme the coordination transformation must be considered. The master and slave robots share the same world coordinate $\{W\}$. At the beginning both master and slave robots are at the initial configurations. When the master robot moves relatively with respect to its initial position the slave robot should behave the same with respect to its initial position. The desired rotational matrix and translational vector of the slave robot are calculated.

Rotational matrix

$$R_{current}^m = \Delta R^m \cdot R_{init}^m \quad (5.2)$$

where ΔR^m is the relative rotational movement of the master tool defined in the world frame. R_{init}^m and $R_{current}^m$ are the initial rotational matrix and the current rotational matrix of the master tool respectively. Therefore, the relative rotational movement of the master tool defined in the world frame is computed as shown below:

$$\Delta R^m = R_{current}^m \cdot (R_{init}^m)^{-1} \quad (5.3)$$

This leads to the desired rotational matrix of the slave robot $R_{desired}^s$ as follows:

$$R_{desired}^s = \Delta R^m \cdot R_{init}^s = R_{current}^m \cdot (R_{init}^m)^{-1} \cdot R_{init}^s \quad (5.4)$$

where R_{init}^s is the initial rotational matrix of the slave robot.

Translational vector

$$p_{init}^m + \Delta p^m = p_{current}^m \quad (5.5)$$

where Δp^m is the relative translational movement of the master tool defined in the world frame. p_{init}^m and $p_{current}^m$ are the initial translational vector and the current translational vector of the master tool respectively. It is simple to deduce from Eq. (5.5) that

$$\Delta p^m = (p_{current}^m) - p_{init}^m \quad (5.6)$$

$$p_{desired}^s = p_{init}^s + \Delta p^m \quad (5.7)$$

where p_{init}^s is the initial translational vector of the slave robot. The desired rotational matrix $R_{desired}^s$ and the translational vector $p_{desired}^s$ will be the reference to the impedance controller of the slave robot.

5.2.2. Force feedback

The wrench including force and torque sensed at the slave robot should be made the same to the master side as well. The wrench measured at the sensor frame $\{SS\}$ of the slave robot is transformed to the end effector frame $\{EE\}$ and then this wrench is transformed to the tool frame $\{T\}$ of the slave robot as follows:

$${}^{EE} \begin{pmatrix} f \\ m \end{pmatrix}_{Slave} = \begin{pmatrix} {}^{EE}R_{SS} & 0 \\ {}^{EE}R_{SS} \cdot {}^{EE}p_{SS} & {}^{EE}R_{SS} \end{pmatrix}^{SS} \begin{pmatrix} f \\ m \end{pmatrix}_{Slave} \quad (5.8)$$

$${}^T \begin{pmatrix} f \\ m \end{pmatrix}_{Slave} = \begin{pmatrix} {}^T R_{EE} & 0 \\ {}^T R_{EE} \cdot {}^E p_{EE} & {}^T R_{EE} \end{pmatrix}^{EE} \begin{pmatrix} f \\ m \end{pmatrix}_{Slave} \quad (5.9)$$

After that the wrench in the tool frame of the slave robot is transformed into the world frame $\{W\}$.

$${}^W \begin{pmatrix} f \\ m \end{pmatrix}_{Slave} = \begin{pmatrix} {}^W R_T & 0 \\ 0 & {}^W R_T \end{pmatrix}^T \begin{pmatrix} f \\ m \end{pmatrix}_{Slave} \quad (5.10)$$

Finally, this wrench is transformed to the tool frame of the master robot.

$${}^T \begin{pmatrix} f \\ m \end{pmatrix}_{Master} = \begin{pmatrix} {}^T R_W & 0 \\ 0 & {}^T R_W \end{pmatrix}^W \begin{pmatrix} f \\ m \end{pmatrix}_{Slave} \quad (5.11)$$

The reason why transformations in Eq. (5.10) and (5.11) are different from what is defined in Eq. (2.19) is that we only want to transfer exactly the wrench sensed at the tool of the slave robot to the tool of the master robot. Therefore, the component in the screw transformation containing moment arm is made to be zero as indicated in Eq. (5.10) and (5.11); otherwise the moment arm can magnify the moment component to a large value due to a large distance from the origin of the world coordinate to the origins of the tool coordinates of the master and slave robots.

Then the torque to be applied to the master robot can be determined by multiplying the wrench in the tool frame with the transpose of the Jacobian matrix J^T :

$$\tau_{feedback} = J^T K_{fb}^T \begin{pmatrix} f \\ m \end{pmatrix}_{Master} \quad (5.12)$$

where K_{fb} is the force feedback gain. In implementation, this gain is chosen by trial and error as $K_{fb} = [0.5 \ 0.5 \ 0.5 \ 0.2 \ 0.2 \ 0.2]$. Therefore, the human operator at the master side can feel the scaled interaction force at the slave side.

5.2.3. Controller design for master robot

The model of the master robot in Cartesian coordinate is given by:

$$\Lambda_m(q_m)\ddot{x}_m + \mu_m(q_m, \dot{q}_m)\dot{x}_m + J(q_m)^{-T}g(q_m) = J(q_m)^{-T}\tau + F_h \quad (5.13)$$

where F_h is the external force caused by human operator. Other notations have similar meanings as Eq. (2.26). The torque computed to control the master robot motors τ comprises two terms. The first one is responsible for gravity compensation while the second one is responsible for force feedback. Therefore, the control law is as follows:

$$\tau = \tau_g + \tau_{feedback}, \quad (5.14)$$

where $\tau_{feedback}$ is the feedback torque which is calculated as Eq. (5.12). When this controller is applied to the master robot the human operator can easily move it and feel the interacting force at the slave side.

5.2.4. Controller design for slave robot

The model of the slave robot in Cartesian coordinate is as follows:

$$\Lambda_s(q_s)\ddot{x}_s + \mu_s(q_s, \dot{q}_s)\dot{x}_s + J(q_s)^{-T}g(q_s) = J(q_s)^{-T}\tau_s + F_h. \quad (5.15)$$

The control law applied to the slave robot is similar to that in Eq. (2.29):

$$\tau_s = g(q_s) + J(q_s)^T(\Lambda(q_s)\ddot{x}_{sd} + \mu(q_s, \dot{q}_s)\dot{x}_s - D_d\dot{\tilde{x}}_s - K_d\tilde{x}_s) \quad (5.16)$$

The meaning of the notations here is the same as in Eq. (2.29). In implementation of the above control law, the inertial force and Coriolis and centrifugal force are practically negligible since they have small effects on the controller performance. This leads to a simplified control law:

$$\tau = g(q_s) + J(q_s)^T(-D_d\dot{\tilde{x}}_s - K_d\tilde{x}_s) \quad (5.17)$$

The desired damping gain D_d is set to constant as [25 25 25 2.5 2.5 2.5]. The damping force can be easily calculated as:

$$F_{damping} = -D_d\dot{\tilde{x}} = -D_dJ(q_s)\dot{q}_s. \quad (5.18)$$

In order to calculate the stiffness force $F_{stiffness} = K_d\tilde{x}_s$ we need a representation of orientation in the space. Roll-Pitch-Yaw angles is chosen to compute this force. Suppose that we know the desired transformation matrix T_d^s and the current transformation T_c^s from the tool coordinate to the world coordinate of the slave robot.

$$T_d^s = \begin{pmatrix} R_{desired}^s & p_{desired}^s \\ 0 & 1 \end{pmatrix} \quad (5.19)$$

$$T_c^s = \begin{pmatrix} R_{current}^s & p_{current}^s \\ 0 & 1 \end{pmatrix} \quad (5.20)$$

The relative transformation matrix between T_d^s and T_c^s is as follows:

$$\Delta T^s = (T_c^s)^{-1}T_d^s \quad (5.21)$$

5. Teleoperation

From this transformation matrix we can compute the translational vector (3×1) and Roll-Pitch- Yaw angles ($\alpha \beta \gamma$) (3×1) which can be combined into a single vector (6×1). The details of the computation can be found in Appendix. This vector represented by \tilde{x} which can be multiplied with the diagonal matrix K_d to produce stiffness force $F_{stiffness}$ as follows:

$$F_{stiffness} = -K_d \cdot \tilde{x} \quad (5.22)$$

where K_d is given as:

$$K_d = \begin{pmatrix} K_x & 0 & 0 & 0 & 0 & 0 \\ 0 & K_y & 0 & 0 & 0 & 0 \\ 0 & 0 & K_z & 0 & 0 & 0 \\ 0 & 0 & 0 & K_\alpha & 0 & 0 \\ 0 & 0 & 0 & 0 & K_\beta & 0 \\ 0 & 0 & 0 & 0 & 0 & K_\gamma \end{pmatrix}. \quad (5.23)$$

The above stiffness K_d can vary according to EMG signals using one of two following methods.

Method 1

$K_x = K_{11}$; $K_y = K_{22}$ which are estimated from EMG signals as Eq. (4.18). Other values $K_z, K_\alpha, K_\beta, K_\gamma$ are constant, $K_z = 1000(N/m)$, $K_\alpha = K_\beta = K_\gamma = 18(Nm/rad)$

Method 2

K_x, K_y, K_z are computed as in section 4.4. $K_\alpha = K_\beta = K_\gamma = 18(Nm/rad)$.

5.3. Results and discussions

When applying calibration methods to the bilateral teleoperation scheme, methods 2 show the behaviour as expected. The scaled stiffness varies according to the sum of all EMG signals as can be seen in the last graph of Fig. 5.2. When the stiffness is too high a saturation is used to prevent this. The maximum possible scaled stiffness is 2000 (N/m). At the beginning, two master and slave robots are placed at initial positions. Then the human operator start doing teleoperation. The relative movement of each robot in X, Y and Z directions with respect to its initial position is shown in first three graphs in Fig. 5.2. We can see that the slave robot can follow the movement of the master robot. Additionally, when the subject releases his arm the scaled stiffness is quite low the position error is relatively large. On the contrary, once he does co-contraction the scaled stiffness is high. This leads to quite small position error of the slave robot.

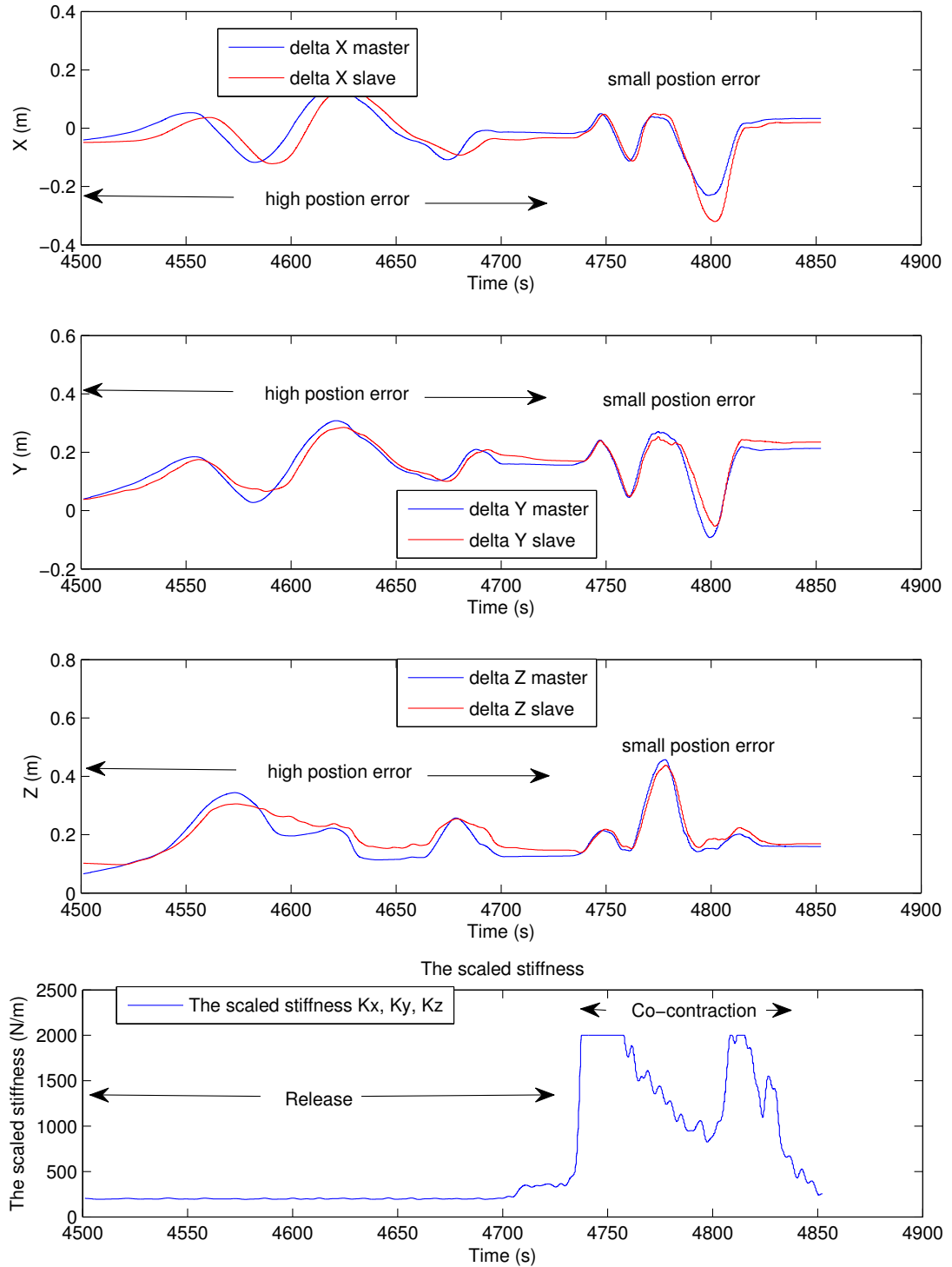


Figure 5.2.: The behaviour of the slave robot with low and high stiffness scaled from EMG signals

6. Conclusion and future works

In this thesis, human arm identification including geometrics, inertial parameters and endpoint stiffness was presented. The geometrics identification is quite repeatable and precise while the inertial parameter identification is just an approximation of the main inertial parameters which primarily contribute to the dynamics of human arm. This is due to the assumptions that each link of human are rigid body with symmetric forms and. A method of using novel force field to measure endpoint stiffness of human arm in 2D with different co-contraction levels is implemented. However, it is very difficult to force the subject do the same co-contraction level with the same force field level. That could make stiffness not consistent for different perturbations with the same force field level. Further more, during the experiment, the subject can learn to reduce the metabolic cost. This is another reason that makes the stiffness measurement varying for the same force field level. Therefore, a further investigation of measuring human arm stiffness for different co-contraction level need to be tackled. One possibility to improve the stiffness measurement is combination of the novel force fields and the measured EMG signals. The perturbation happens only when the EMG signals of certain muscles in a certain range and the subject fulfils the task.

Consequently, the calibration between endpoint stiffness in 2D and EMG signals is presented. With good measured data using Regularized Least Squares method stiffness proves to be estimated quite stably at the calibrated location. Additionally, a simple method to scale the stiffness according to EMG signals is also discussed. This allows to compute online endpoint stiffness from EMG signals without mechanical perturbation.

Finally, a bilateral teleoperation scheme using EMG-based impedance controller is implemented. The slave robot is controlled by Cartesian impedance controller which varies stiffness according to EMG signals from human operator. This allows the human operator to flexibly change the stiffness of the slave robot to fulfil the requirements of interaction. Further investigation of stability of the bilateral teleoperation scheme with time delay should be considered.

The main limitation of this thesis is that the calibration works only locally. The calibration should be done for all regions in the workspace of the arm. However, that will increase the calibration time dramatically. Another possibility to improve is using inverse geometrics of human arm and combine it with joint stiffness in order to estimate the endpoint stiffness in workspace of human arm in plane. The method can be expanded into 3D in order not to limit the working range of bilateral teleoperation.

Appendix

A. Results of geometric identification

Table A.1.: Joint position identification result 2

	${}^1d_{1S}$	${}^2d_{2S}$	${}^2d_{2E}$	${}^3d_{3E}$
x (m)	-0.066	-0.222	0.067	-0.200
y (m)	-0.534	0.0308	-0.025	0.015
z (m)	0.661	-0.032	-0.024	-0.014

Table A.2.: Joint position identification result 3

	${}^1d_{1S}$	${}^2d_{2S}$	${}^2d_{2E}$	${}^3d_{3E}$
x (m)	-0.082	-0.217	0.068	-0.198
y (m)	-0.565	0.054	-0.022	0.012
z (m)	0.647	-0.033	-0.031	-0.022

Table A.3.: Joint position identification result 4

	${}^1d_{1S}$	${}^2d_{2S}$	${}^2d_{2E}$	${}^3d_{3E}$
x (m)	0.079	-0.213	0.070	-0.196
y (m)	-0.544	0.038	-0.021	0.013
z (m)	0.639	-0.041	-0.031	-0.024

Table A.4.: Joint position identification result 5

	${}^1d_{1S}$	${}^2d_{2S}$	${}^2d_{2E}$	${}^3d_{3E}$
x (m)	-0.085	-0.220	0.069	-0.197
y (m)	-0.557	0.049	-0.021	0.008
z (m)	0.629	-0.042	-0.032	-0.024

Table A.5.: Joint position identification result 6

	${}^1d_{1S}$	${}^2d_{2S}$	${}^2d_{2E}$	${}^3d_{3E}$
x (m)	-0.076	-0.228	0.069	-0.197
y (m)	-0.553	0.054	-0.024	0.012
z (m)	0.662	-0.037	-0.019	-0.007

B. Calculation of Roll-Pitch-Yaw angles from rotational matrix

$$R = \text{rot}(z, \alpha) \text{rot}(y, \beta) \text{rot}(x, \gamma)$$

$$\alpha = \text{atan2}(R_{32}, R_{33})$$

$$\beta = \text{atan2}(R_{21}, R_{11})$$

$$\gamma = \text{atan2}(-R_{31}, \sqrt{R_{21}^2 + R_{11}^2})$$

List of Figures

1.1. Tele-manipulation applications	1
1.2. The simulation of DEOS project [6]	2
1.3. The animal motions	3
1.4. The human motions	4
1.5. The interaction control in robots	4
1.6. EMG-based control	5
2.1. The impedance controller principle [26]	11
3.1. The human arm model [27]	14
3.2. The joint identification approach [27]	15
3.3. The placement of marker sets	15
3.4. The geometric parameters and the transformations in geometric identification [27]	18
3.5. Geometrics identification setup	19
3.6. Link model	21
3.7. Forces and moments on link j [14]	22
3.8. Configurations 1 and 2	23
3.9. Changes of torque when the subject is moving his arm from configuration 1 to 2	24
3.10. Configuration 3	24
3.11. Changes of torque when the subject is moving his arm from configuration 1 to 3	25
3.12. The overview of the system	28
3.13. EMG electrode placement [27]	29
3.14. The perturbation profile	30
3.15. The divergent force field	32
3.16. The velocity force field [17]	32
3.17. The graphical representation to the subjects	33
3.18. The subject position	34
3.19. The position of the arm in the cuff	34
3.20. The whole procedure of stiffness measurement	35
3.21. The perturbation characteristics	37
3.22. The stiffness ellipses for different co-contraction levels of subject 1	39
3.23. The stiffness for different co-contraction levels of subject 2	40
3.24. The indication of learning in control stiffness. Four outside ellipses are earlier stiffness while four inside ellipses are the later stiffness	41
4.1. The raw EMG signal of one channel	42

4.2. The processed EMG	43
4.3. The EMG signals (number according to the Table 3.6 at page 28)	44
4.4. The processed EMG signals	47
4.5. The estimated stiffness from EMG signals using Least Squares Regression	49
4.6. The estimated stiffness from EMG signals using Regularized Least Squares $\lambda_{11} = 0.001, \lambda_{12} = 0.001, \lambda_{21} = 0.001, \lambda_{22} = 0.001$	51
4.7. The estimated stiffness from EMG signals using Regularized Least Squares $\lambda_{11} = 0.0005, \lambda_{12} = 0.0005, \lambda_{21} = 0.0005, \lambda_{22} = 0.0005$	52
5.1. EMG based bilateral controller [24]	55
5.2. The behaviour of the slave robot with low and high stiffness scaled from EMG signals	59

List of Tables

3.1. The start predefined arm configurations	19
3.2. The final predefined arm configurations	20
3.3. Joint position identification result	20
3.4. The arm configurations for inertial parameter identification	23
3.5. The measured inertial parameters	25
3.6. EMG electrodes [27]	29
3.7. The symmetric components of Cartesian stiffness matrix of subject 1	38
3.8. The anti-symmetric components of Cartesian stiffness matrix of subject 1	38
3.9. The symmetric components of Cartesian stiffness matrix of subject 2	38
3.10. The anti-symmetric components of Cartesian stiffness matrix of subject 2	38
4.1. The correlation value between stiffness elements and EMG signals	45
A.1. Joint position identification result 2	63
A.2. Joint position identification result 3	63
A.3. Joint position identification result 4	63
A.4. Joint position identification result 5	63
A.5. Joint position identification result 6	63

Bibliography

- [1] care-o-bot can take good care of you. <http://www.tuvie.com/care-o-bot-can-take-good-care-of-you/>. Accessed: 2014-02-25.
- [2] Cheetah. <http://www.yoyowall.com/wp-content/uploads/2013/04/Cheetah-Jump.jpg>. Accessed: 2014-02-25.
- [3] Driving bicycle. <http://sportsrecreationdomains.blogspot.de/>. Accessed: 2014-02-25.
- [4] The falling cat. <http://blog.uvm.edu/cgoodnig/2013/12/26/group-selection-and-religion/>. Accessed: 2014-02-25.
- [5] Ice skating. <http://www.olympic.org/photos/figure-skating-ice-dance-free-dance-meryl-davis-charlie-white-usa-gold-medallists-1>. Accessed: 2014-02-25.
- [6] Raumfahrtrobotik, Technologien und Einsatzbereiche. <http://www.schuldorf.de/source/aktuelles/highlights13/weltraumabend/wra.html>. Accessed: 2014-02-25.
- [7] C. Ott A. Stemmer T. Wimboeck A. Albu-Schäffer, S. Haddadin and G. Hirzinger. The DLR lightweight robot: design and control concepts for robots in human environments. *Industrial Robot: An International Journal*, 34(5):376–385, 2007.
- [8] A. Ajoudani, N. Tsagarakis, and A. Bicchi. Tele-impedance: Teleoperation with impedance regulation using a body-machine interface. *Int. J. Rob. Res.*, 31(13):1642–1656, October 2012.
- [9] Alin Albu-Schäffer. Cartesian Impedance Control of Redundant Robots : Recent Results with the DLR-Light-Weight-Arms.
- [10] Alin Albu-Schäffer and Gerd Hirzinger. Cartesian impedance control techniques for torque controlled light-weight robots. *Proc. 2002 IEEE Int. Conf. Robot. Autom. (Cat. No.02CH37292)*, 1(May):657–663, 2002.
- [11] Alexander. Elastic energy stores in running vertebrates. *Zoology*, 24(2):85–94, 1984.
- [12] A.V.Hill. The heat of shortening and the dynamic constants of muscle. *Biological Science*, 5(2), 1938.
- [13] Paolo de Leva. Adjustments to zatsiorsky-seluyanov’s segment inertia parameters. *Journal of Biomechanics*, 29(9):1223 – 1230, 1996.
- [14] W.Khalil E.Dombre. *Modeling, Identification and Control of Robots*. Hermes Penton Ltd, 2002.

- [15] A.A. Frolov M. Mokhtari E.V. Biryukova, A. Roby-Brami. Kinematics of human arm reconstructed from spatial tracking system recordings. *Biomechanics*, 33(2):985–995, 2000.
- [16] David W Franklin, Etienne Burdet, Rieko Osu, Mitsuo Kawato, and Theodore E Milner. Functional significance of stiffness in adaptation of multijoint arm movements to stable and unstable dynamics. *Exp. Brain Res.*, 151(2):145–157, July 2003.
- [17] David W. Franklin, Rieko Osu, Etienne Burdet, Mitsuo Kawato, and Theodore E Milner. Adaptation to stable and unstable dynamics achieved by combined impedance control and inverse dynamics model. *J. Neurophysiol.*, 90(5):3270–82, November 2003.
- [18] Arjan Gijberts. Incremental learning for robotics with constant update complexity, 2011. Doctor Thesis.
- [19] U. Hagn, R. Konietzschke, A. Tobergte, M. Nickl, S. Jörg, B. Kübler, G. Passig, M. Gröger, F. Fröhlich, U. Seibold, L. Le-Tien, A. Albu-Schäffer, A. Nothhelfer, F. Hacker, M. Grebenstein, and G. Hirzinger. DLR MiroSurge: a versatile system for research in endoscopic telesurgery. *Int. J. Comput. Assist. Radiol. Surg.*, 5(2):183–93, March 2010.
- [20] N. Hogan. Adaptive control of mechanical impedance by coactivation of antagonist muscles. *IEEE Trans. Automat. Contr.*, 29(8):681–690, August 1984.
- [21] Neville Hogan. An organizing principle for a class of voluntary movements. *The Journal of Neuroscience*, 4(11):2745–2754, 1984.
- [22] Neville Hogan. The mechanics of multi-joint posture and movement control. *Biological Cybernetics*, 52(5):315–331, 1985.
- [23] Peter F. Hokayem and Mark W. Spong. Bilateral teleoperation: An historical survey. *Automatica*, 42(12):2035–2057, December 2006.
- [24] Claudio Castellini Alin Albu-Schäffer Jordi Artigas, Albert Arquer. Emg based teleoperation with force feedback. 2013.
- [25] Hyun K. Kim, Byungduk Kang, Byungchan Kim, and Shinsuk Park. Estimation of Multijoint Stiffness Using Electromyogram and Artificial Neural Network. *IEEE Trans. Syst. Man, Cybern. - Part A Syst. Humans*, 39(5):972–980, September 2009.
- [26] Dominic Lakatos. Identifikation der impedanzparameter des menschlichen arms mit dem sieben-achs dlr leichtbauroboter. Master’s thesis, Munich University, May 2011. Available from <http://elib.dlr.de/>.
- [27] Marvin Ludersdofer. Mechanical properties of human arm: Modelling and identification, 2012.
- [28] N.Hogan Mussa Ivaldi and E.Bizzi. Neural, Mechanical, and Geometric Factors subserving Arm Posture in Humans. *Neuroscience*, 5(2):2732–2743, 1985.

- [29] Christian Ott. *Cartesian Impedance Control of Redundant and Flexible-Joint Robots*. Springer, 2008.
- [30] C. Castellini Partrick van der Smagt, J. Vogel. EMG-Based Teleoperation and Manipulation with the DLR LWR-III. *IEEE*, 2011.
- [31] Claudio Castellini Partrick van der Smagt. Surface EMG in advanced hand prosthetics. *Biological Cybernetics*, 2008.
- [32] Jacquelin Perry and GA Bekey. EMG-force relationships in skeletal muscle. *Crit Rev Biomed Eng*, 1981.
- [33] Rolf Pfeifer and Josh Bongard. *How the body shapes the way we think*. The MIT press, 2007.
- [34] Duk Shin, Jaehyo Kim, and Yasuharu Koike. A myokinetic arm model for estimating joint torque and stiffness from EMG signals during maintained posture. *J. Neurophysiol.*, 101(1):387–401, January 2009.